Molecular Cell
Short Article

Structure of a Blm10 Complex Reveals Common Mechanisms for Proteasome Binding and Gate Opening

Kianoush Sadre-Bazzaz,[1] Frank G. Whitby,[1] Howard Robinson,[2] Tim Formosa,[1] and Christopher P. Hill[1,*]
[1]Department of Biochemistry, University of Utah School of Medicine, Salt Lake City, UT 84112-5650, USA
[2]Biology Department, Brookhaven National Laboratory, Upton, NY 11973-5000, USA
*Correspondence: chris@biochem.utah.edu
DOI 10.1016/j.molcel.2010.02.002

SUMMARY

The proteasome is an abundant protease that is critically important for numerous cellular pathways. Proteasomes are activated in vitro by three known classes of proteins/complexes, including Blm10/PA200. Here, we report a 3.4 Å resolution crystal structure of a proteasome-Blm10 complex, which reveals that Blm10 surrounds the proteasome entry pore in the 1.2 MDa complex to form a largely closed dome that is expected to restrict access of potential substrates. This architecture and the observation that Blm10 induces a disordered proteasome gate structure challenge the assumption that Blm10 functions as an activator of proteolysis in vivo. The Blm10 C terminus binds in the same manner as seen for 11S activators and inferred for 19S/PAN activators and indicates a unified model for gate opening. We also demonstrate that Blm10 acts to maintain mitochondrial function. Consistent with the structural data, the C-terminal residues of Blm10 are needed for this activity.

INTRODUCTION

The bulk of proteolysis in the cytosol and nucleus of eukaryotes is performed by an ~700 kDa barrel-shaped protease called the proteasome (20S proteasome, also referred to as core particle [CP]), whose activity is important for protein quality control and the regulation of many biological pathways (Glickman and Ciechanover, 2002). Proteasomes comprise 28 protein subunits assembled into four heptameric rings, with outer rings composing α subunits and inner rings β subunits, to form a hollow complex that sequesters the proteolytic sites at the N termini of β subunits (Groll et al., 1997; Löwe et al., 1995; Seemüller et al., 1995). The seven distinct α subunits (α1–7) and seven distinct β subunits (β1–7) of eukaryotic proteasomes each occupy a unique position in their respective rings (Groll et al., 1997; Unno et al., 2002). Substrates enter the proteasome through a pore at the center of the α subunit ring that is closed in the absence of an activator by interactions among the N-terminal peptides of α subunits, with α2, α3, and α4 making the major contributions to closing the gate.

Three classes of activator facilitate substrate access to the proteasome interior by binding α subunits. The 11S activators, PA28/REG/PA26, are heptameric rings that, as revealed by proteasome-PA26 crystal structures (Förster et al., 2003, 2005; Whitby et al., 2000), stimulate the hydrolysis of peptides by stabilizing an ordered open conformation of the entrance pore. The C termini of 11S activators bind in pockets between proteasome α subunits through main-chain to main-chain hydrogen bonds and a salt bridge between the C-terminal carboxylate and proteasome Lys66 (*T. acidophilum* proteasome numbering is used throughout). To open the gate, 11S activators utilize an internal "activation loop" (Zhang et al., 1998), which repositions the Pro17 reverse turns of proteasome α subunits to destabilize the closed conformation and allow formation of a fully open conformation. Biochemical studies indicate that the unrelated PAN/19S activator induces the same open conformation as PA26 (Förster et al., 2003) and utilizes a similar mode of binding (Förster et al., 2005), although PAN/19S appears to lack an activation loop and achieves both binding and gate opening through interactions of C-terminal residues (Gillette et al., 2008; Rabl et al., 2008; Smith et al., 2007).

Unlike the oligomeric 11S and PAN/19S activators, which use multiple C termini to bind in pockets between α subunits, Blm10 (Fehlker et al., 2003; Iwanczyk et al., 2006; Schmidt et al., 2005), previously known as Blm3 (Doherty et al., 2004), and its mammalian homolog PA200 (Ustrell et al., 2002) are single-chain proteins of 2143 residues (~250 kDa, *S. cerevisiae* sequence). Blm10 and PA200 are predominantly nuclear and stimulate the degradation of model peptides, although they do not appear to stimulate the degradation of proteins, recognize ubiquitin, or utilize ATP. The mouse PA200 knockout displays a defect in spermatogenesis (Khor et al., 2006), and roles in DNA repair and genomic stability have been proposed (Blickwedehl et al., 2007, 2008; Ustrell et al., 2002). Studies in yeast have produced inconsistent data that suggest roles in proteasome assembly/maturation (Fehlker et al., 2003; Marques et al., 2007) and proteasome inhibition (Lehmann et al., 2008), whereas early indications of bleomycin sensitivity were not supported by later studies, which found no role for Blm10 in the repair of DNA damage induced by bleomycin or other factors (Iwanczyk et al., 2006).

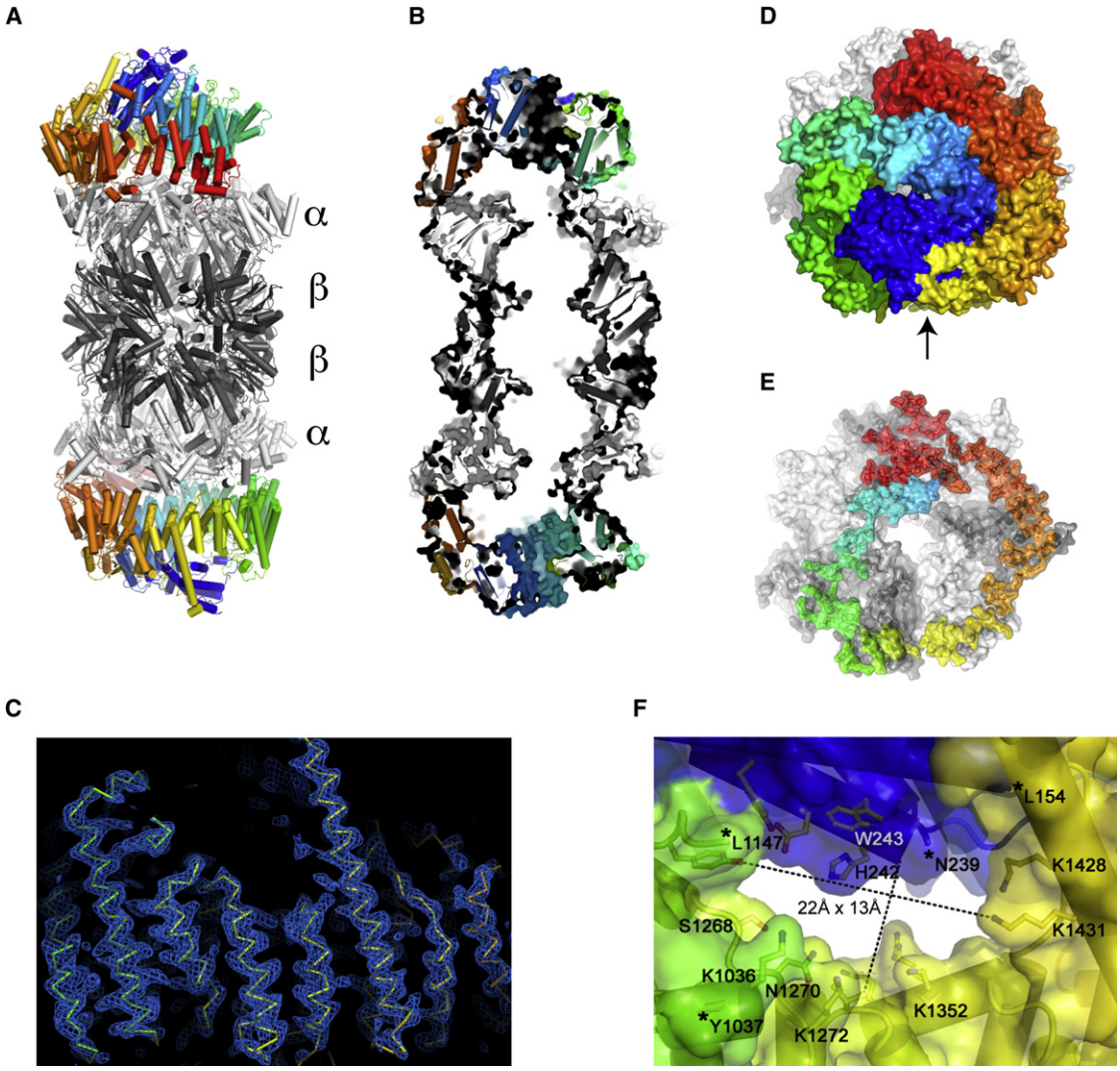

Figure 1. Structure of the Blm10:Proteasome Complex

(A) Cartoon of the Blm10:proteasome complex, side view. Proteasome white (α subunits) and gray (β subunits), Blm10 rainbow from N terminus (blue) to C terminus (red).

(B) Cutaway view with the molecular surface.

(C) Electron density for Blm10. All maps shown in this paper were phased on the proteasome molecular replacement model for which segments approaching Blm10 had been removed. The phases were refined by solvent flattening, histogram shifting, and 4-fold noncrystallographic symmetry averaging.

(D) Top view, space-filling representation. The opening visible in the center of this view measures only ~6 Å between atom centers. The largest opening, which is not visible in this orientation, is indicated with an arrow.

(E) Same as (D) but only showing Blm10 residues that have at least one atom within 6 Å of the proteasome.

(F) Close-up view of the largest opening through the Blm10 dome. Orientation as indicated by the arrow in (D). Asterisks denote the last-ordered residues adjacent to disordered segments that have been omitted from the model.

In order to better understand Blm10 mechanism, we have determined the crystal structure of a proteasome complex. The results challenge the model that Blm10 is a proteasome activator in vivo and also indicate that binding by 11S, 19S/PAN, and PA200/Blm10 is more similar than previously realized. We further report that yeast cells lacking Blm10 fail to maintain normal levels of mitochondrial function and that this phenotype also results when just the C-terminal residues that make contacts between Blm10 and the proteasome are deleted.

RESULTS AND DISCUSSION

Blm10-Proteasome Structure Determination

We determined a 3.4 Å crystal structure of the *S. cerevisiae* proteasome capped on both ends by Blm10 (Figure 1 and Figure S1 available online) to an R_{free} of 25% (Table 1). A variety of Blm10 constructs were screened, and several crystal forms were obtained, with the best data collected from a construct that lacked the first 50 residues of Blm10, which are poorly

Table 1. Proteasome:Blm10 Crystallographic Data Statistics

Crystallographic Data						
ID/name[a]	c158/FL-1	c164/FL-thim	c172/FL-$PtCl_4$	c280/NΔ50-1	c290/NΔ50-MeHg	c292/NΔ50-$PtCl_4$
Spacegroup	$P2_12_12_1$	$P2_1$	$P2_12_12_1$	$P2_1$	$P2_1$	$P2_1$
Cell						
a (Å)	124.1	238.2	128	236.1	238.7	237.8
b (Å)	238.5	126.2	236.2	127.8	127.8	128.6
c (Å)	489.8	528.7	515.1	532.3	535.6	537.1
β (Å)		102.5		102.8	102.5	102.8
Resolution (Å)[b]	50–3.9 (4.0–3.9)	40–6.2 (6.4–6.2)	50–6.0 (6.2–6.0)	30–3.4 (3.5–3.4)	30–6.8 (7.0–6.8)	30–6.8 (7.0–6.8)
R_{merge} (%)	20.9 (42.8)	11.0 (43.6)	18.2 (58.3)	10.3 (31.4)	9.6 (36.5)	9.4 (35.9)
I/σ(I)	6.3 (2.2)	8.6 (2.1)	9.3 (2.4)	10.3 (2.4)	9.7 (2.0)	9.4 (2.1)
Completeness	98.2 (97.3)	99.6 (99.9)	99.2 (97.7)	98.6 (88.6)	99.8 (99.6)	99.8 (99.9)
Refinement Statistics						
Resolution (Å)[b]				30–3.0		
# reflns used in refinement[c]				490,961		
R_{work}/R_{free} (%)				19.6/25.0		
Number of atoms[c]				158,904		
<B> ($Å^2$)				104.3		
Rmsd bond lengths(Å)[d]				0.01		
Rmsd bond angles (°)				1.291		

Values in parentheses refer to the high-resolution shell.

[a] Each data set was collected from a single crystal, which was given a unique identifier and a more descriptive name. Crystals were of full-length (FL) Blm10 or Blm10 missing the first 50 amino acid residues (Δ50). Mercury (Hg)- or platinum (Pt)-heavy atom derivatives were prepared as described in the Supplemental Experimental Procedures.

[b] Resolution of a data set was formally defined as the Bragg spacing at which half of the measured reflections have an I/σ(I) value of at least 2.0, although the data were processed and used to smaller Bragg spacing. All crystallographic data values in this table refer to reflections within the formal resolution limits, whereas the refinement statistics refer to all data.

[c] The total number of all 20S and Blm10 nonhydrogen atoms in the asymmetric unit. No solvent molecules were included in the model.

[d] Rmsd denotes root mean square deviation from ideality.

conserved and predicted to be disordered. The ordered regions of Blm10 seen in the structure are residues 79–154, 239–1037, and 1147–2143 (C terminus), consistent with proteolytic cleavage observed by SDS-PAGE and N-terminal sequencing upon storage at 4°C (Iwanczyk et al., 2006) and in crystals (data not shown). A number of observations argue that the crystal structure is not unduly influenced by lattice contacts (Figures S1A–S1D), including the very large Blm10-proteasome interface that includes all seven α subunits and buries more than 10,000 $Å^2$ of solvent-accessible surface area (Figure 1E).

Overall Structure Description

Blm10 encodes 32 HEAT repeat (HR)-like modules (Kajava et al., 2004), each comprising two helices joined by a turn, with adjacent repeats connected by a linker (Figures 1 and S1E). The first ordered Blm10 residue, Thr79, lies ~60 Å above the proteasome surface and is followed by three short helices and loops before starting HR1 at His133. The following HEAT repeats continue almost to the C terminus and spiral through a 1.5 turn left-handed solenoid to form a dome that encloses a volume of ~110,000 $Å^3$ above the proteasome. Whereas a standard HEAT repeat is composed of ~50 residues, the Blm10 HEAT repeats are highly variable. The length of helices ranges from 8 to 35 residues, turns range from 2 to 87 residues, and linkers range from 1 to 88 residues, with the longest linker, between HR21 and HR22, containing additional secondary structures (two strands and three helices).

Restricted Opening through the Blm10 Dome

The extensive Blm10 interface surrounds the proteasome entrance pore (Figure 1E). Consistent with the observation that Blm10/PA200 stimulates the hydrolysis of small peptides, but not proteins, the largest opening through the Blm10 dome is only 13 Å by 22 Å when measured between atomic nuclei (Figure 1F). Moreover, access may be further restricted because segments of Blm10 that are not visible in the structure connect residues Leu154 to Asn239 and Tyr1037 to Leu1147, which are all adjacent to the mouth of the opening. A biological rationale for Blm10/PA200 to facilitate peptide hydrolysis in vivo is not obvious, and the structure is consistent with suggestions that Blm10 functions in proteasome assembly (Fehlker et al., 2003; Marques et al., 2007), as an adaptor (Rechsteiner and Hill, 2005) or as a physiological inhibitor (Lehmann et al., 2008). We cannot discount the possibilities that unfolded proteins might access the proteasome through this pore, perhaps with the assistance of an as yet unidentified ATPase or that substrate

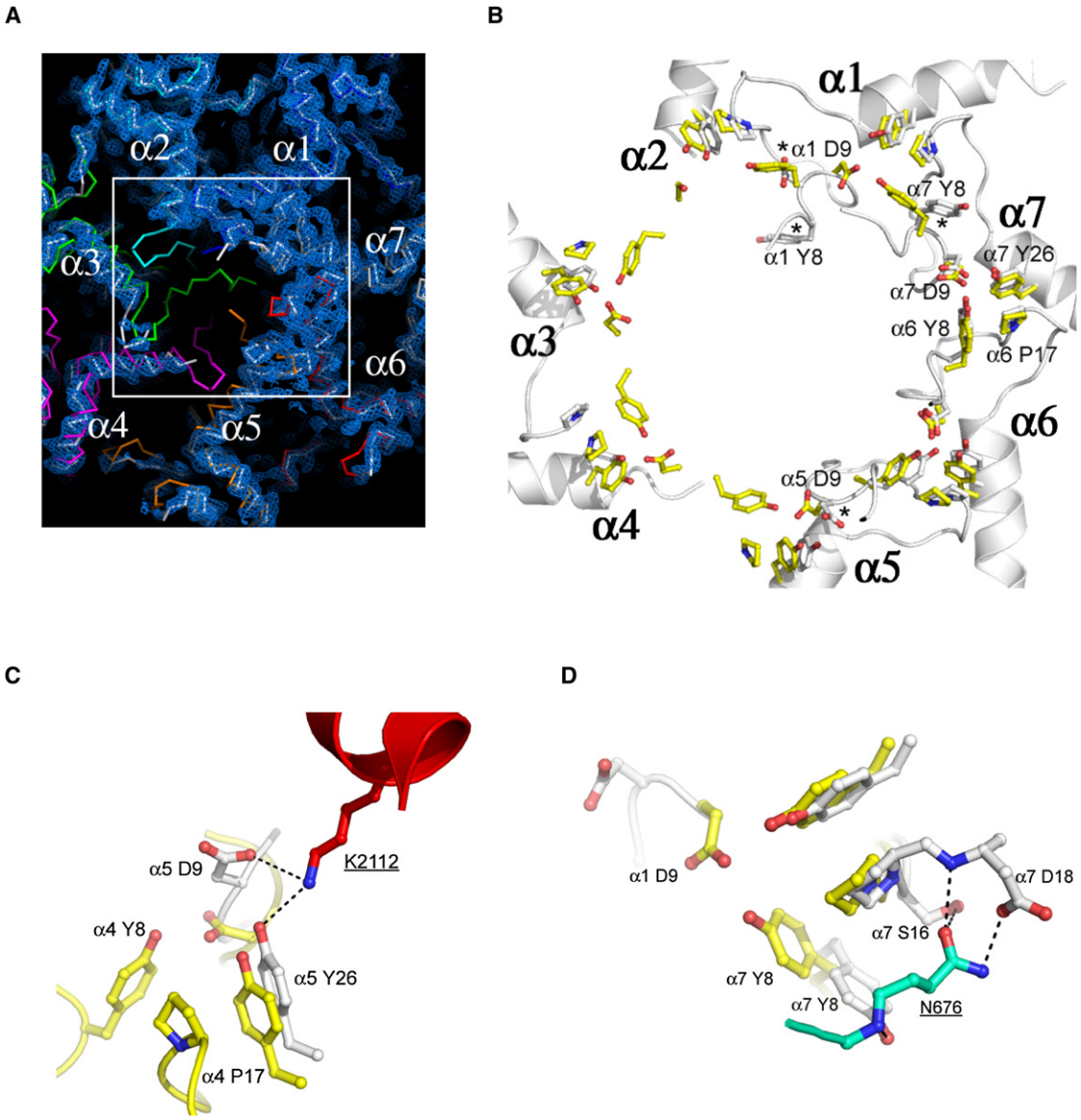

Figure 2. Proteasome Conformational Changes Induced by Blm10

(A) Top view of the proteasome pore region with electron density for the Blm10 complex. The absence of density for the N-terminal residues of proteasome α2, α3, and α4 indicates that they are disordered in the Blm10 complex (white), whereas they are ordered in the closed, unliganded conformation (colors) and in the fully open complex with PA26 (not shown in this panel).

(B) Open conformation seen in complexes with PA26 (yellow) and Blm10 (white). The stabilizing cluster residues (Tyr8, Asp9, Pro17, and Tyr26 [Förster et al., 2003]) are labeled for the α6/α7 cluster, which is ordered in the unliganded proteasome (Groll et al., 1997) and in both the PA26 and Blm10 complexes shown here. Tyr8 and Asp9 residues are not ordered for α2, α3, or α4 in the Blm10 complex. Residues indicated with an asterisk are ordered in the Blm10 complex but are displaced from the open conformation seen with PA26. A version of this panel that also includes the closed conformation is shown in Figure S2.

(C) Contacts that stabilize α5Asp9 away from the open conformation.

(D) Contacts that stabilize α7Tyr8 away from the open conformation.

proteins might be bound within the Blm10 dome prior to proteasome association.

The Proteasome Gate Is Disordered

The proteasome β subunits do not move discernibly upon binding Blm10 (rmsd = 0.4 Å on all Cα atoms), whereas the α subunits move somewhat toward the open conformation seen in complexes with PA26 to form a pore that is disordered rather than fully open or fully closed (Figure 2). This flexible conformation is expected to allow passage of small model substrates but to impede access of larger substrates (Benaroudj et al., 2003; Förster et al., 2003). Both the dome architecture and the proteasome pore conformation are therefore consistent with biochemical studies indicating that Blm10 and PA200

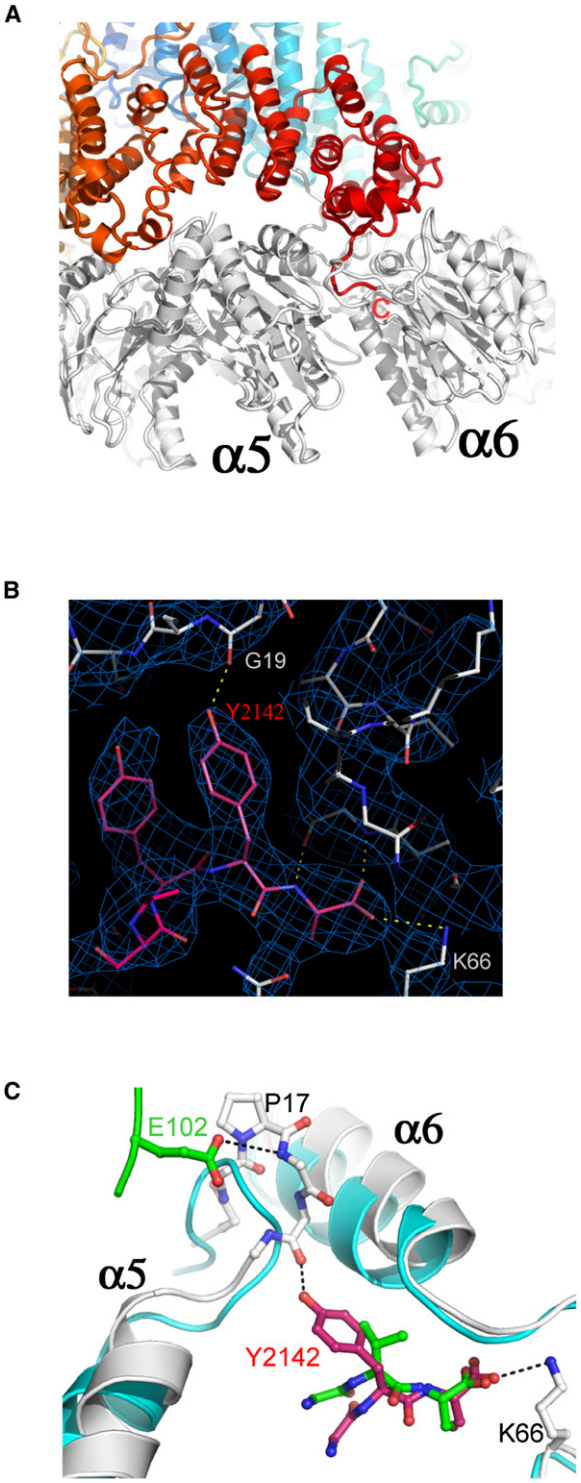

Figure 3. Interactions of the Blm10 C-Terminal Residues

(A) Side view with Blm10 C terminus labeled "C."

(B) The electron density map is well defined for the Blm10 penultimate tyrosine (Tyr2142) and surrounding residues.

(C) The last three residues of PA26 (green) and Blm10 (red) are shown after overlap of the two complexes on surrounding proteasome residues. Unliganded proteasome (Groll et al., 1997), cyan. Blm10 Tyr2142 stabilizes the open position of α5 by hydrogen bonding with Gly19 O. PA26 stabilizes the same transition by hydrogen bonding interactions of its activation loop residue Glu102.

stimulate the hydrolysis of peptides, but not proteins (Iwanczyk et al., 2006; Schmidt et al., 2005; Ustrell et al., 2002).

It is instructive to compare the proteasome complexes with Blm10 and PA26. The fully open conformation results from repositioning of the seven proteasome α subunit Pro17 turns by the PA26 activation loop to form a wider, more circular arrangement, with the largest Pro17 Cα movement (3.6 Å) seen for α4 and the smallest Pro17 Cα movement (0.4 Å) seen for α1 (Förster et al., 2003). Repositioning of the Pro17 turns induces ordering of the Tyr8 and Asp9 residues of all seven proteasome α subunits to form a continuous belt around the pore circumference that is stabilized by conserved clusters of Tyr8, Asp9, Pro17, and Tyr26 proteasome residues (Figure 2B) (notwithstanding the noncanonical α1/α2 cluster [Förster et al., 2003]). Blm10 stabilizes the same Pro17 transition for proteasome α5 as seen with PA26, although it does so primarily by interactions of its C-terminal residues rather than by an internal activation loop. In contrast, the Pro17 turns of α2, α3, and α4 lack direct contacts with Blm10 and become disordered. Moreover, Blm10 blocks the fully open conformation by displacing α5Asp9 from a position where it could bind α4Tyr8 (Figure 2C) and by displacing α7Tyr8 from a position where it could bind α1Asp9 (Figure 2D). This explains why α1 and α4, and hence their contacting α2 and α3 subunits, do not form the same open conformation as seen with PA26.

Implications for Binding and Gate Opening by 19S/PAN

The C-terminal residues of Blm10 bind in the pocket between proteasome α5 and α6 in a conformation that superimposes with the C-terminal residues of PA26 (Figure 3). PA26 is heptameric and binds to all seven pockets of the 7-fold symmetric archaeal *T. acidophilum* proteasome and to four (α2/α3, α3/α4, α4/α5, α5/α6) pockets of the *S. cerevisiae* proteasome (Förster et al., 2005). Like PA26, the Blm10 C-terminal residues form β sheet-like hydrogen bonds with the proteasome, and the Blm10 C-terminal carboxylate forms a salt bridge with α6Lys66. Of interest, biochemical (Förster et al., 2005; Smith et al., 2007) and electron microscopic (Rabl et al., 2008) data indicate that the C termini of some of the 19S/RC activator ATPases and their archaeal homolog PAN also bind to the same site, presumably using the same interactions.

In contrast to the apparently shared mode of binding by 11S, Blm10/PA200, and 19S/PAN, an important difference is that peptides corresponding to the seven C-terminal residues of PAN and some 19S subunits are able to both bind proteasomes and stabilize the open gate conformation (Gillette et al., 2008; Rabl et al., 2008; Smith et al., 2007), whereas PA26/11S use their C-terminal sequences for binding but rely upon a distantly located activation loop to induce gate opening. Furthermore, a critical interaction for proteasome gate opening has been mapped to the penultimate tyrosine of PAN/19S ATPases, with some of the homologs containing a phenylalanine at this position (Gillette et al., 2008; Smith et al., 2007). Remarkably, the penultimate residue of Blm10, Tyr2142, is also invariably conserved as tyrosine or phenylalanine in an alignment of 46 sequences (Figure S1E). This residue possesses well-defined electron

density in the Blm10:proteasome structure, and the side chain reaches from the C-terminal binding site to hydrogen bond with the oxygen atom of α5Gly19 and stabilize the adjacent α5Pro17 reverse turn in the same open gate conformation as seen in proteasome complexes with PA26 (Figure 3C). Presumably, the penultimate tyrosine of PAN/19S subunits makes the same interactions as seen for the penultimate tyrosine of Blm10, with the monomeric Blm10 moving a single proteasome α subunit Pro17 turn and disordering the gate and the oligomeric PAN/19S moving multiple α subunits to induce a fully open gate conformation. This model calls into question the proposal that PAN/19S induces gate opening without making direct contacts to the Pro17 turn (Rabl et al., 2008) and is consistent with a recent report that the penultimate tyrosine or phenylalanine of chimeric PA26 complexes designed to model the PAN/19S-proteasome interaction display equivalent contacts (Stadtmueller et al., 2009). Thus, although important questions remain, we favor the model that Blm10/PA200, 11S, and 19S/PAN all bind through their C-terminal residues and partially or fully open the proteasome gate by displacing one or multiple Pro17 turns, with Blm10 and PAN/19S using a penultimate tyrosine/phenylalanine to move the Pro17 turn and PA26/11S using an internal activation loop.

Blm10 Is Important for Maintenance of Mitochondrial Function

Several genetic links have been reported between Blm10 and proteasome function, including synthetic growth defects in cells lacking both Blm10 and Ecm29 or Rpn4 (Schmidt et al., 2005) or lacking both Blm10 and the C terminus of Pre4/β7 (Marques et al., 2007). We have been unable to confirm the interactions with Ecm29 (Iwanczyk et al., 2006) or Pre4, although we have observed genetic interactions between *blm10* and *rpn4* mutations (Figure S3A), supporting a role for Blm10 in a proteasome-related process.

We now report that deletion of *BLM10* causes yeast cells to lose mitochondrial function at a high frequency (Figure 4). In the A364a genetic background, a strain with a deletion of the entire *BLM10* gene yields about 9-fold more petite derivatives than a strain with normal Blm10. These cells are unable to grow on glycerol media because they lack the functional mitochondria required to metabolize this nonfermentable carbon source. This requirement is not specific to A364a cells because the yield of petites is significantly elevated for *blm10*-Δ mutants in three other commonly used backgrounds (Figure 4B).

Other mutations that cause defects in proteasome function have also been reported to cause increased levels of petite formation, although the mechanisms linking proteasomes to this phenotype remain under investigation and may be diverse. For example, loss of the 20S assembly chaperone Ump1 causes elevated levels of petite formation (Malc et al., 2009). This has been attributed to mitochondrial DNA damage due to increased production of reactive oxygen species (ROS) coupled with diminished levels of DNA repair (Malc et al., 2009). We therefore tested *blm10*-Δ deletion strains for increased ROS levels using a dihydrofluorescein diacetate assay (Malc et al., 2009) but found only a small, statistically insignificant increase (Figure S3B). Also unlike *UMP1*, deletion of *BLM10* causes only a small increase in the yield of erythromycin resistant mutants

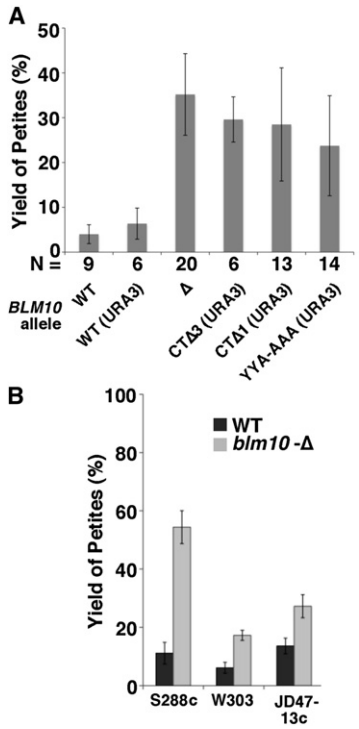

Figure 4. The C-Terminal Residues of Blm10 Are Important for Its Function

(A) Isogenic strains were constructed in the A364a genetic background with the genotypes indicated (Table S1). Multiple independent colonies of each strain growing on glycerol medium to select for retention of mitochondrial function were used to inoculate rich medium containing glucose. Saturated cultures were diluted and plated on rich glucose medium, and then mitochondrial function in clones was assessed using the tetrazolium staining method (Ogur et al., 1957). Results from multiple strains with the same genotype were combined (Table S1, total number indicated as N), with the average percentage yield of petite colonies plotted here. Error bars indicate the standard deviation of the measurements.

(B) As in (A), except isogenic pairs from three other commonly used genetic backgrounds containing or lacking Blm10 were assayed by picking 120 colonies without regard to size and then replica plating to media containing glycerol or glucose to determine the number of petite colonies (Table S1). See also Figure S3.

(Figure S3B), which arise through mutation of a mitochondrial rDNA gene. Furthermore, deletion of *BLM10* causes a small increase in the mRNA encoding the DNA repair protein Msh1 (D. Stillman and Y. Yu, personal communication), whereas deletion of *UMP1* is reported to show a 4-fold decrease (Malc et al., 2009). These data indicate that Blm10 and Ump1 employ distinct mechanisms for the maintenance of mitochondrial function.

Mutation of the 19S subunit Rpn11 also causes petite formation, although, in this case, the mechanism appears to involve mislocalization or aberrant persistence of factors that promote mitochondrial tubulation or that otherwise regulate fission and fusion, as these mutants display abnormal mitochondrial fragmentation (Rinaldi et al., 2008). The morphology of the mitochondria in *blm10*-Δ mutants appears to be normal, indicating a different mechanism for petite formation than that occurring in *rpn11* mutants (data not shown).

The C Terminus of Blm10 Is Important for Its Physiological Function

To test the importance of the conserved C terminus of Blm10, we deleted the last three codons (TyrTyrAla) in the normal genomic context. Consistent with the observation that these residues make intimate contact with the proteasome but do not contact other Blm10 residues, this mutant was as stable as the intact protein (Figure S3C) and localized to the nucleus in a manner indistinguishable from WT (data not shown). The truncated protein failed to maintain normal levels of mitochondrial function, and the yield of petites was similar to that obtained with a complete deletion of *BLM10* (Figure 4A). Other perturbations of the C terminus, including deletion of just the last residue or mutation of the YYA sequence to AAA, also caused severe impairment of Blm10 function (Figure 4A). These demonstrations that the C terminus of Blm10 performs a physiologically important function are consistent with our structural finding that these residues play a specific role in proteasome binding and definition of the gate conformation.

Conclusions

We have verified that Blm10 functions in a proteasome-related process and have demonstrated that it is required for the maintenance of mitochondrial function by a mechanism that is distinct from that of previously reported genes. We have also determined the structure of Blm10 in complex with the proteasome and found an unexpected similarity in binding by C-terminal residues, which indicates common modes of proteasome binding for Blm10, 11S, and 19S/PAN. Of note, the penultimate tyrosine residue makes specific interactions that suggest a refinement of current models for binding and gate opening by 19S/PAN activators. Consistent with the structure, genetic analysis indicates that the C-terminal residues of Blm10 are required for its physiological function. Despite these advances, a number of important questions remain. For example, we do not yet understand the role of Blm10 in maintaining mitochondrial vitality, although this phenotype provides both a conceptual rationale for the conservation of Blm10 among eukaryotes and an assay to probe the effect of mutating the *BLM10* gene on a physiologically important function of Blm10. We also note that, in view of the high abundance of mitochondria in spermatozoa, it is attractive to speculate that a role in maintaining mitochondrial function underlies the requirement of the mammalian Blm10 homolog PA200 for spermatogenesis (Khor et al., 2006). The structure appears somewhat at odds with Blm10s characterization as a proteasome activator in vitro and seems more consistent with possible functions as an adaptor, assembly factor, or inhibitor. Thus, whereas fundamentally important questions of Blm10 biology remain to be answered, the structure and genetic demonstration of a role in maintaining mitochondrial function provide tools and insight that can guide future studies.

EXPERIMENTAL PROCEDURES

See the Supplemental Information for a more complete description of the methods. Double-capped *S. cerevisiae* proteasome:Blm10 and Δ50Blm10 complexes were prepared largely as described (Iwanczyk et al., 2006). Protein was concentrated to 20–25 mg/ml for crystallization by vapor diffusion. Diffraction data were collected at 100K at the National Synchrotron Light Source beamline X29 and were phased by molecular replacement using the unliganded proteasome (Groll et al., 1997) (PDB code: 1ryp) as the search model.

ACCESSION NUMBERS

Coordinates and diffraction data have been deposited at the Protein Data Bank with accession code 3L5Q.

SUPPLEMENTAL INFORMATION

Supplemental Data include Supplemental Experimental Procedures, three figures, and one table and can be found with this article online at doi:10.1016/j.molcel.2010.02.002.

ACKNOWLEDGMENTS

We thank Charisse Kettelkamp and Hua Xin for technical assistance, Pavel Afonine for running Phenix calculations, Heidi Schubert for assistance and advice on aspects of the crystallography, Daniel Finley and David Legett for providing the yeast strain sDL135 that expresses the protein A-tagged Pre1 proteasome subunit, David Stillman and Yaxin Yu for *MSH1* mRNA data, and Martin Rechsteiner and Beth Stadtmueller for critical comments on the manuscript. We gratefully acknowledge the DNA Synthesis and Sequencing Core Facilities at the University of Utah. X-ray diffraction data for this study were measured at beamline X29 of the National Synchrotron Light Source (NSLS). Financial support for NSLS comes principally from the Offices of Biological and Environmental Research and of Basic Energy Sciences of the US Department of Energy and from the National Center for Research Resources of the National Institutes of Health. This work was supported by National Institutes of Health Grant RO1 GM059135.

Received: June 29, 2009
Revised: November 9, 2009
Accepted: December 29, 2009
Published: March 11, 2010

REFERENCES

Benaroudj, N., Zwickl, P., Seemüller, E., Baumeister, W., and Goldberg, A.L. (2003). ATP hydrolysis by the proteasome regulatory complex PAN serves multiple functions in protein degradation. Mol. Cell *11*, 69–78.

Blickwedehl, J., McEvoy, S., Wong, I., Kousis, P., Clements, J., Elliott, R., Cresswell, P., Liang, P., and Bangia, N. (2007). Proteasomes and proteasome activator 200 kDa (PA200) accumulate on chromatin in response to ionizing radiation. Radiat. Res. *167*, 663–674.

Blickwedehl, J., Agarwal, M., Seong, C., Pandita, R.K., Melendy, T., Sung, P., Pandita, T.K., and Bangia, N. (2008). Role for proteasome activator PA200 and postglutamyl proteasome activity in genomic stability. Proc. Natl. Acad. Sci. USA *105*, 16165–16170.

Doherty, K., Pramanik, A., Pride, L., Lukose, J., and Moore, C.W. (2004). Expression of the expanded YFL007w ORF and assignment of the gene name BLM10. Yeast *21*, 1021–1023.

Fehlker, M., Wendler, P., Lehmann, A., and Enenkel, C. (2003). Blm3 is part of nascent proteasomes and is involved in a late stage of nuclear proteasome assembly. EMBO Rep. *4*, 959–963.

Förster, A., Whitby, F.G., and Hill, C.P. (2003). The pore of activated 20S proteasomes has an ordered 7-fold symmetric conformation. EMBO J. *22*, 4356–4364.

Förster, A., Masters, E.I., Whitby, F.G., Robinson, H., and Hill, C.P. (2005). The 1.9 A structure of a proteasome-11S activator complex and implications for proteasome-PAN/PA700 interactions. Mol. Cell *18*, 589–599.

Gillette, T.G., Kumar, B., Thompson, D., Slaughter, C.A., and DeMartino, G.N. (2008). Differential roles of the COOH termini of AAA subunits of PA700 (19 S

regulator) in asymmetric assembly and activation of the 26 S proteasome. J. Biol. Chem. *283*, 31813–31822.

Glickman, M.H., and Ciechanover, A. (2002). The ubiquitin-proteasome proteolytic pathway: destruction for the sake of construction. Physiol. Rev. *82*, 373–428.

Groll, M., Ditzel, L., Löwe, J., Stock, D., Bochtler, M., Bartunik, H.D., and Huber, R. (1997). Structure of 20S proteasome from yeast at 2.4 A resolution. Nature *386*, 463–471.

Iwanczyk, J., Sadre-Bazzaz, K., Ferrell, K., Kondrashkina, E., Formosa, T., Hill, C.P., and Ortega, J. (2006). Structure of the Blm10-20 S proteasome complex by cryo-electron microscopy. Insights into the mechanism of activation of mature yeast proteasomes. J. Mol. Biol. *363*, 648–659.

Kajava, A.V., Gorbea, C., Ortega, J., Rechsteiner, M., and Steven, A.C. (2004). New HEAT-like repeat motifs in proteins regulating proteasome structure and function. J. Struct. Biol. *146*, 425–430.

Khor, B., Bredemeyer, A.L., Huang, C.Y., Turnbull, I.R., Evans, R., Maggi, L.B., Jr., White, J.M., Walker, L.M., Carnes, K., Hess, R.A., and Sleckman, B.P. (2006). Proteasome activator PA200 is required for normal spermatogenesis. Mol. Cell. Biol. *26*, 2999–3007.

Lehmann, A., Jechow, K., and Enenkel, C. (2008). Blm10 binds to pre-activated proteasome core particles with open gate conformation. EMBO Rep. *9*, 1237–1243.

Löwe, J., Stock, D., Jap, B., Zwickl, P., Baumeister, W., and Huber, R. (1995). Crystal structure of the 20S proteasome from the archaeon T. acidophilum at 3.4 A resolution. Science *268*, 533–539.

Malc, E., Dzierzbicki, P., Kaniak, A., Skoneczna, A., and Ciesla, Z. (2009). Inactivation of the 20S proteasome maturase, Ump1p, leads to the instability of mtDNA in Saccharomyces cerevisiae. Mutat. Res. *669*, 95–103.

Marques, A.J., Glanemann, C., Ramos, P.C., and Dohmen, R.J. (2007). The C-terminal extension of the beta7 subunit and activator complexes stabilize nascent 20 S proteasomes and promote their maturation. J. Biol. Chem. *282*, 34869–34876.

Ogur, M., St. John, R., and Nagai, S. (1957). Tetrazolium overlay technique for population studies of respiration deficiency in yeast. Science *125*, 928–929.

Rabl, J., Smith, D.M., Yu, Y., Chang, S.C., Goldberg, A.L., and Cheng, Y. (2008). Mechanism of gate opening in the 20S proteasome by the proteasomal ATPases. Mol. Cell *30*, 360–368.

Rechsteiner, M., and Hill, C.P. (2005). Mobilizing the proteolytic machine: cell biological roles of proteasome activators and inhibitors. Trends Cell Biol. *15*, 27–33.

Rinaldi, T., Hofmann, L., Gambadoro, A., Cossard, R., Livnat-Levanon, N., Glickman, M.H., Frontali, L., and Delahodde, A. (2008). Dissection of the carboxyl-terminal domain of the proteasomal subunit Rpn11 in maintenance of mitochondrial structure and function. Mol. Biol. Cell *19*, 1022–1031.

Schmidt, M., Haas, W., Crosas, B., Santamaria, P.G., Gygi, S.P., Walz, T., and Finley, D. (2005). The HEAT repeat protein Blm10 regulates the yeast proteasome by capping the core particle. Nat. Struct. Mol. Biol. *12*, 294–303.

Seemüller, E., Lupas, A., Stock, D., Löwe, J., Huber, R., and Baumeister, W. (1995). Proteasome from Thermoplasma acidophilum: a threonine protease. Science *268*, 579–582.

Smith, D.M., Chang, S.C., Park, S., Finley, D., Cheng, Y., and Goldberg, A.L. (2007). Docking of the proteasomal ATPases' carboxyl termini in the 20S proteasome's alpha ring opens the gate for substrate entry. Mol. Cell *27*, 731–744.

Stadtmueller, B.M., Ferrell, K., Whitby, F.G., Heroux, A., Robinson, H., Myszka, D.G., and Hill, C.P. (2009). Structural models for interactions between the 20S proteasome and its PAN/19S activators. J. Biol. Chem. *285*, 13–17.

Unno, M., Mizushima, T., Morimoto, Y., Tomisugi, Y., Tanaka, K., Yasuoka, N., and Tsukihara, T. (2002). The structure of the mammalian 20S proteasome at 2.75 A resolution. Structure *10*, 609–618.

Ustrell, V., Hoffman, L., Pratt, G., and Rechsteiner, M. (2002). PA200, a nuclear proteasome activator involved in DNA repair. EMBO J. *21*, 3516–3525.

Whitby, F.G., Masters, E.I., Kramer, L., Knowlton, J.R., Yao, Y., Wang, C.C., and Hill, C.P. (2000). Structural basis for the activation of 20S proteasomes by 11S regulators. Nature *408*, 115–120.

Zhang, Z., Clawson, A., Realini, C., Jensen, C.C., Knowlton, J.R., Hill, C.P., and Rechsteiner, M. (1998). Identification of an activation region in the proteasome activator REGalpha. Proc. Natl. Acad. Sci. USA *95*, 2807–2811.

Molecular Cell, *Volume 37*

Supplemental Information

Structure of a Blm10 Complex Reveals Common Mechanisms for Proteasome Binding and Gate Opening

Kianoush Sadre-Bazzaz, Frank G. Whitby, Howard Robinson, Tim Formosa, and Christopher P. Hill

Figure S1, related to Figure 1

A number of observations argue that the crystal structure is not unduly influenced by lattice contacts. First, the four Blm10 complexes in the asymmetric unit are closely similar to each other and to reconstructions by electron cryomicroscopy (Iwanczyk et al., 2006; Ortega et al., 2005). Second, conserved residues mediate stabilizing contacts between Blm10 segments that are distant in amino acid sequence (panel A). Third, Blm10 wraps around the end of the proteasome barrel to contact all seven proteasome α-subunits in an interface that buries more than 10,000 $Å^2$ of solvent accessible surface area (Figure 1E) and largely defines the Blm10 conformation. Fourth, a cluster of conserved residues from HR6 to HR9 and from HR30 to beyond HR32, contact each other and residues near the N-terminus of proteasome subunits α5 and α6 (panels B-D) to help define the pore conformation and define the relative orientations of the upper and lower turns of the Blm10 solenoid. Fifth, the 3.4Å crystal structure described here of the complex with Blm10 lacking the first 50 residues appears identical to the crystal structures of full-length Blm10 complexes with proteasome observed in two different crystal forms at lower (4.0Å and 4.4Å) resolution (data not shown).

(A) Blm10 (white) with selected linker segments that stabilize the structure (color). The close-up views illustrate the role of conserved residues (underlined, panel E) that make stabilizing interactions.
(B) Proteasome α5 and α6 N-terminal residues (black) are extended and make extensive contacts with Blm10, including residues that are conserved and also stabilize the relative orientation of the two tiers of the Blm10 solenoid.
(C) Stereoview showing details of α5 N-terminal residues and their contacts. Conserved residues are underlined.
(D) Same as panel D, but for α6 contacts.

(E) *S. cerevisiae* Blm10 sequence. Secondary structures (above) colored as in Figure 1. HEAT repeat helices are labeled 1A for helix A of HEAT repeat 1, etc. Residues disordered in the structure are indicated with a dashed line. Residues that approach the proteasome within 4.0 Å are marked with a square below; contact to α1 blue, α2 cyan, α3 green, α4 magenta, α5 orange, α6 red, α7 gray. Residues identical in *S. cerevisiae* Blm10 and human PA200 are underlined. Blm10 residues conserved in an alignment of 46 related sequences are shown on a yellow background. Conservation is defined according to the ESPript consensus (Gouet et al., 1999) from the automatic alignment, with a few residues also defined as conserved because simple manual adjustment of gaps aligns residues that appear to be structurally important.

Proteasome residues have been highly conserved throughout evolution, especially on the α-subunit surface, with 82/112 (73%) of the proteasome residues that contact Blm10 being identical in *S. cerevisiae* and human. In contrast, the Blm10 sequence is much more divergent, with only 162/2143 (8%) of the residues conserved in the alignment indicated here. The conservation is somewhat higher at the proteasome interface, especially for residues that contact proteasome α5 and α6 subunits, where 17/62 (27%) of Blm10 residues contacting these subunits are conserved.

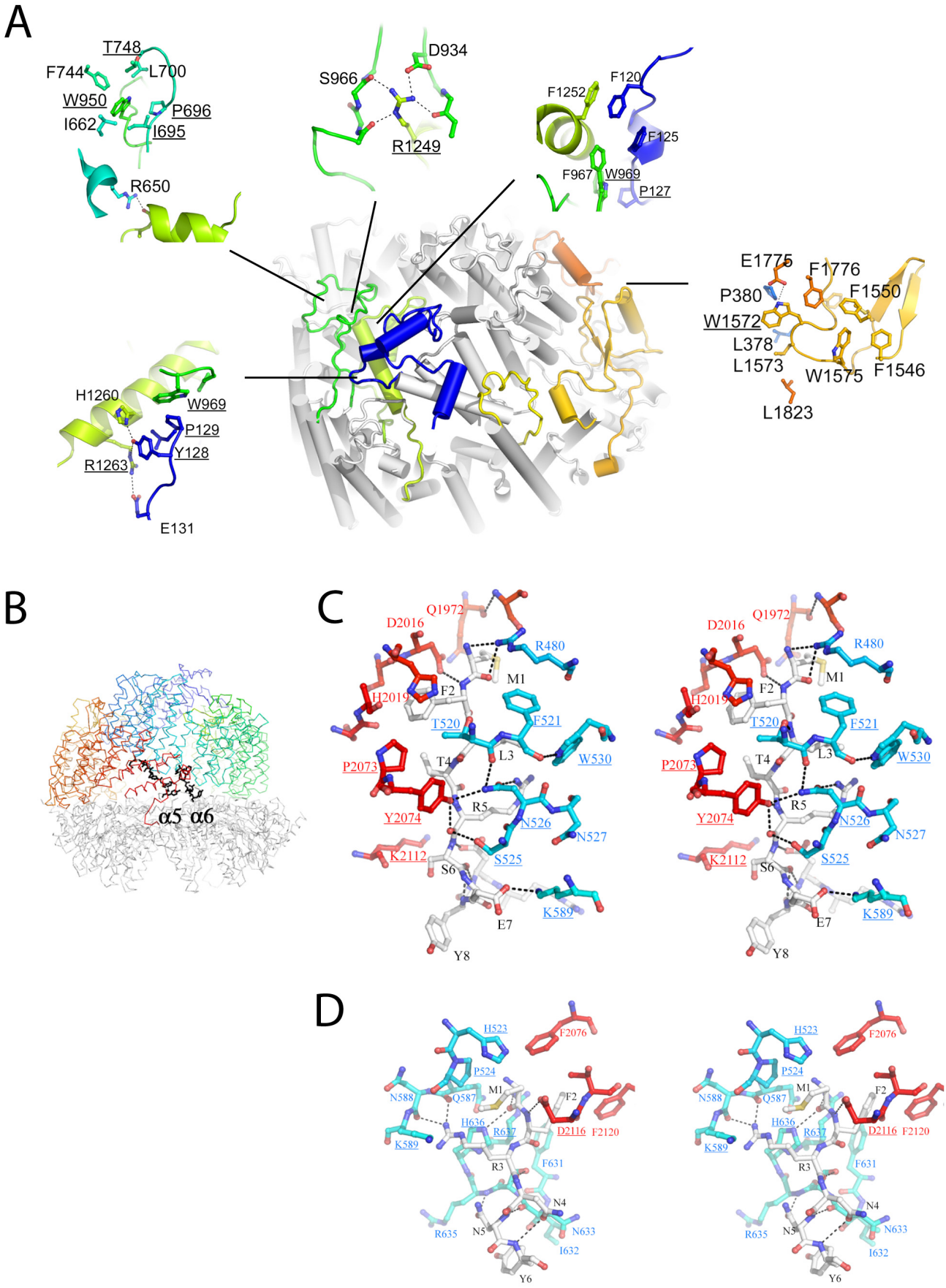
A
T748
F744
L700
W950
P696
I662
I695
R650
S966
D934
R1249
F1252
F120
F125
F967
W969
P127
E1775
F1776
P380
F1550
W1572
L378
L1573
W1575
F1546
L1823
H1260
W969
P129
Y128
R1263
E131
B
α5 α6
C
Q1972
D2016
R480
M1
F2
H2019
T520
F521
L3
W530
P2073
T4
R5
Y2074
N526
N527
K2112
S6
S525
K589
E7
Y8
D
H523
F2076
P524
N588
Q587
M1
F2
H636
R637
D2116
F2120
K589
R3
F631
N4
R635
N5
N633
I632
Y6

E

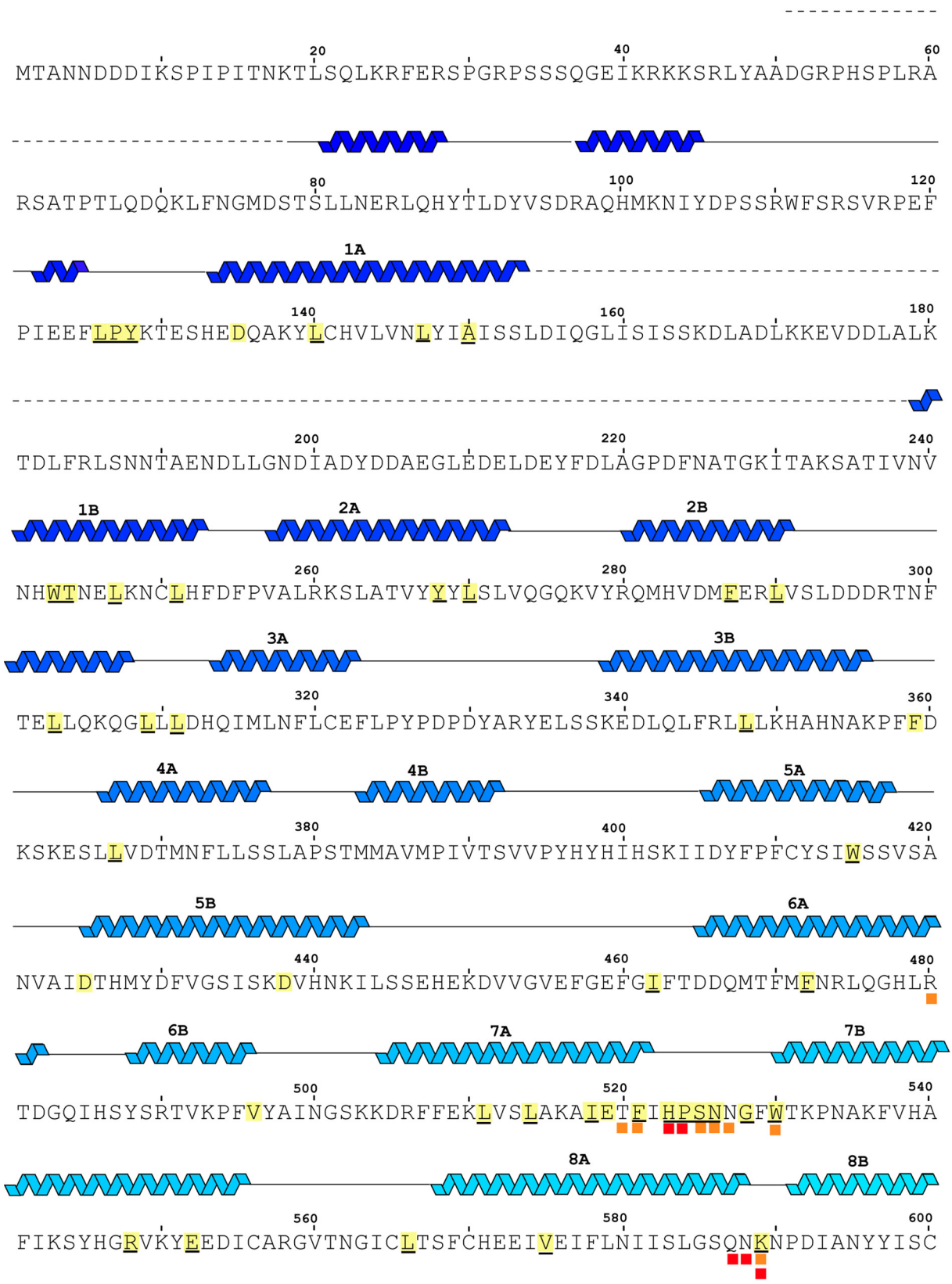
20
40
60
MTANNDDDIKSPIPITNKTLSQLKRFERSPGRPSSSQGEIKRKKSRLYAADGRPHSPLRA
80
100
120
RSATPTLQDQKLFNGMDSTSLLNERLQHYTLDYVSDRAQHMKNIYDPSSRWFSRSVRPEF
1A
140
160
180
PIEEFLPYKTESHEDQAKYLCHVLVNLYIAISSLDIQGLISISSKDLADLKKEVDDLALK
200
220
240
TDLFRLSNNTAENDLLGNDIADYDDAEGLEDELDEYFDLAGPDFNATGKITAKSATIVNV
1B
2A
2B
260
280
300
NHWTNELKNCLHFDFPVALRKSLATVYYYLSLVQGQKVYRQMHVDMFERLVSLDDDRTNF
3A
3B
320
340
360
TELLQKQGLLLDHQIMLNFLCEFLPYPDPDYARYELSSKEDLQLFRLLLKHAHNAKPFFD
4A
4B
5A
380
400
420
KSKESLLVDTMNFLLSSLAPSTMMAVMPIVTSVVPYHYHIHSKIIDYFPFCYSIWSSVSA
5B
6A
440
460
480
NVAIDTHMYDFVGSISKDVHNKILSSEHEKDVVGVEFGEFGIFTDDQMTFMFNRLQGHLR
6B
7A
7B
500
520
540
TDGQIHSYSRTVKPFVYAINGSKKDRFFEKLVSLAKAIETFIHPSNNGFWTKPNAKFVHA
8A
8B
560
580
600
FIKSYHGRVKYEEDICARGVTNGICLTSFCHEEIVEIFLNIISLGSQNKNPDIANYYISC

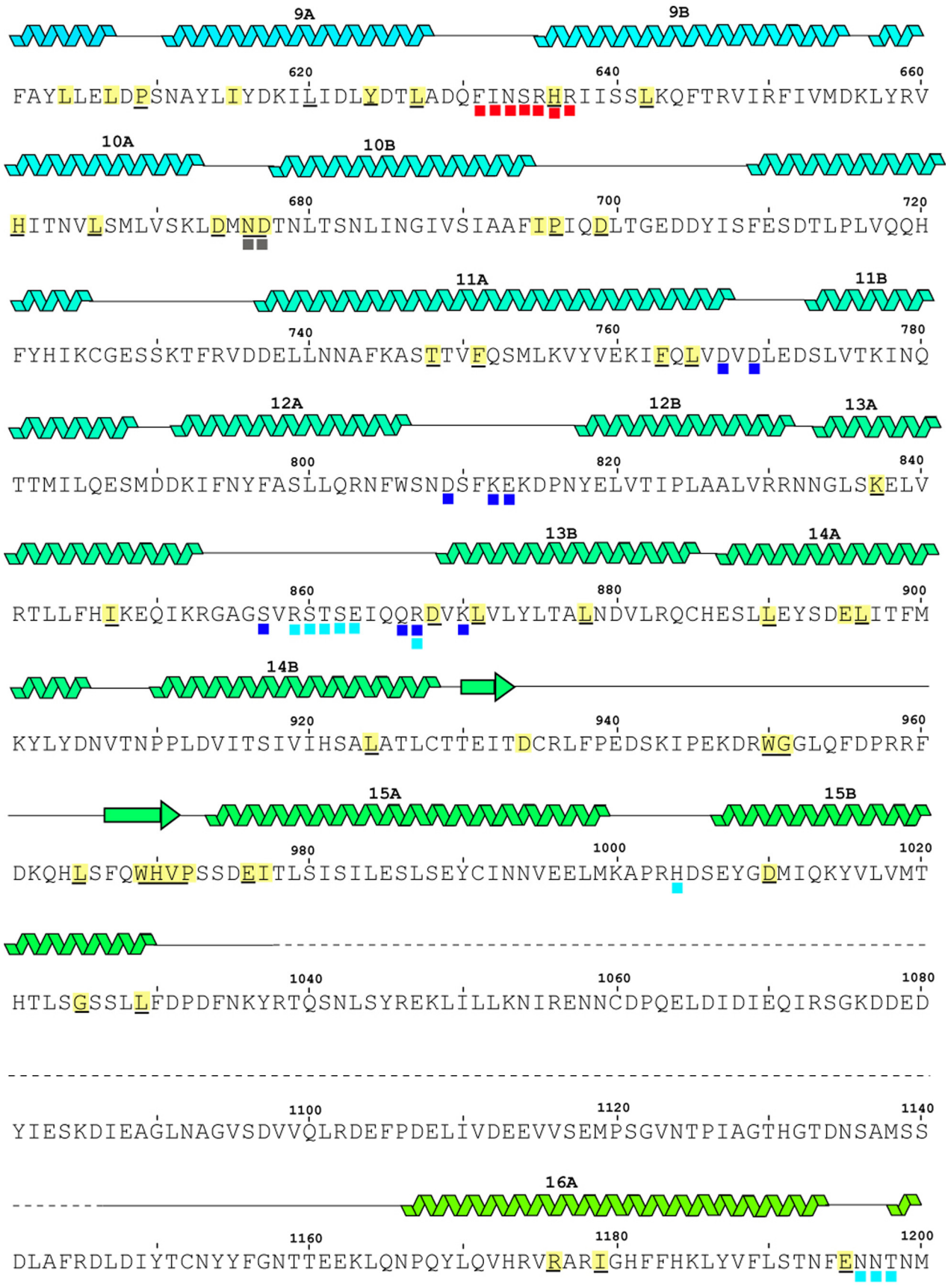
9A
9B
620
640
660
FAYLLELDPSNAYLIYDKILIDLYDTLADQFINSRHRIISSLKQFTRVIRFIVMDKLYRV
10A
10B
680
700
720
HITNVLSMLVSKLDMNDTNLTSNLINGIVSIAAFIPIQDLTGEDDYISFESDTLPLVQQH
11A
11B
740
760
780
FYHIKCGESSKTFRVDDELLNNAFKASTTVFQSMLKVYVEKIFQLVDVDLEDSLVTKINQ
12A
12B
13A
800
820
840
TTMILQESMDDKIFNYFASLLQRNFWSNDSFKEKDPNYELVTIPLAALVRRNNGLSKELV
13B
14A
860
880
900
RTLLFHIKEQIKRGAGSVRSTSEIQQRDVKLVLYLTALNDVLRQCHESLLEYSDELITFM
14B
920
940
960
KYLYDNVTNPPLDVITSIVIHSALATLCTTEITDCRLFPEDSKIPEKDRWGGLQFDPRRF
15A
15B
980
1000
1020
DKQHLSFQWHVPSSDEITLSISILESLSEYCINNVEELMKAPRHDSEYGDMIQKYVLVMT
1040
1060
1080
HTLSGSSLLFDPDFNKYRTQSNLSYREKLILLKNIRENNCDPQELDIDIEQIRSGKDDED
1100
1120
1140
YIESKDIEAGLNAGVSDVVQLRDEFPDELIVDEEVVSEMPSGVNTPIAGTHGTDNSAMSS
16A
1160
1180
1200
DLAFRDLDIYTCNYYFGNTTEEKLQNPQYLQVHRVRARIGHFFHKLYVFLSTNFENNTNM

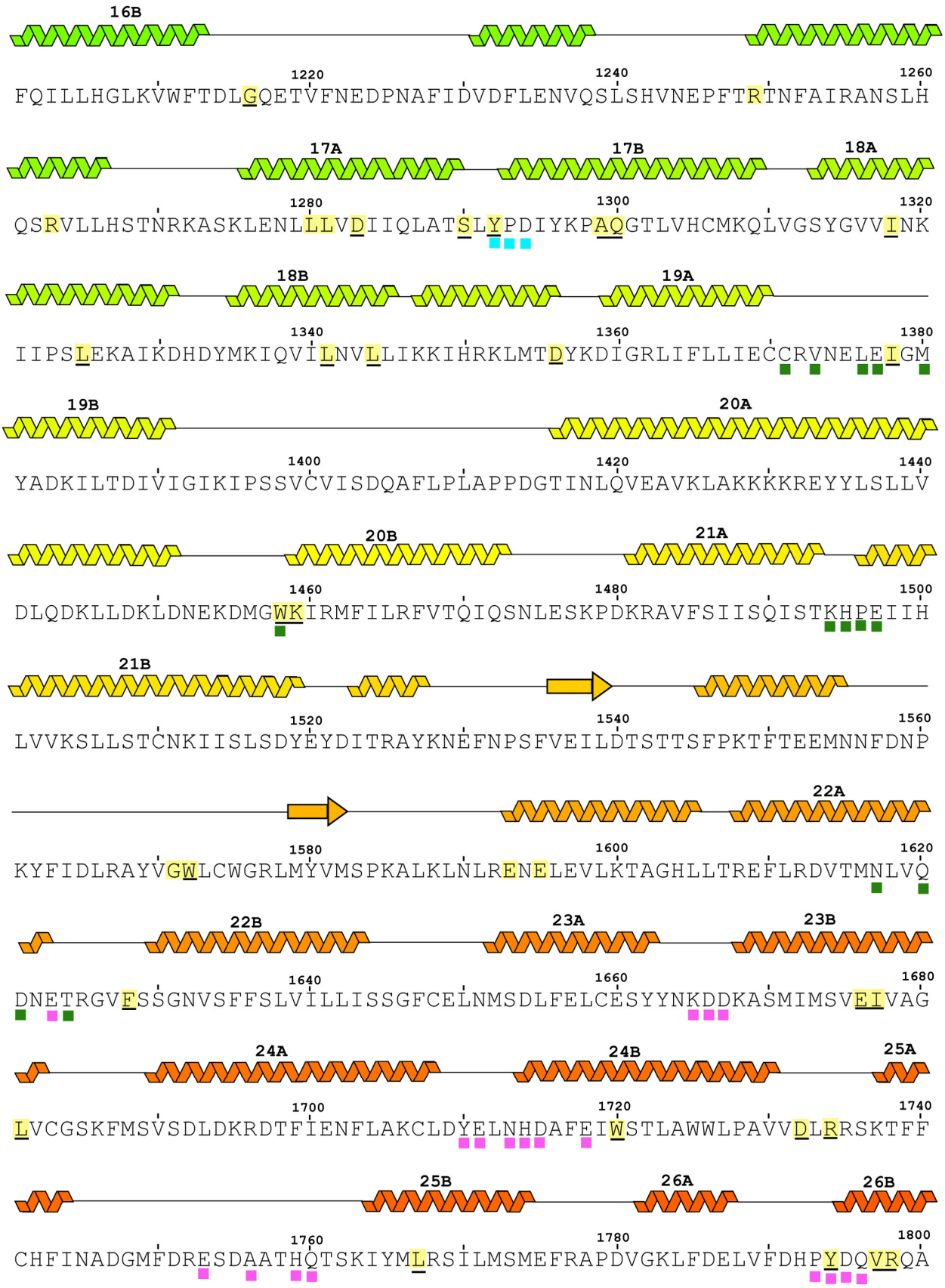
16B
1220
1240
1260
FQILLHGLKVWFTDLGQETVFNEDPNAFIDVDFLENVQSLSHVNEPFTRTNFAIRANSLH
17A
17B
18A
1280
1300
1320
QSRVLLHSTNRKASKLENLLLVDIIQLATSLYPDIYKPAQGTLVHCMKQLVGSYGVVINK
18B
19A
1340
1360
1380
IIPSLEKAIKDHDYMKIQVILNVLLIKKIHRKLMTDYKDIGRLIFLLIECCRVNELEIGM
19B
20A
1400
1420
1440
YADKILTDIVIGIKIPSSVCVISDQAFLPLAPPDGTINLQVEAVKLAKKKKREYYLSLLV
20B
21A
1460
1480
1500
DLQDKLLDKLDNEKDMGWKIRMFILRFVTQIQSNLESKPDKRAVFSIISQISTKHPEIIH
21B
1520
1540
1560
LVVKSLLSTCNKIISLSDYEYDITRAYKNEFNPSFVEILDTSTTSFPKTFTEEMNNFDNP
22A
1580
1600
1620
KYFIDLRAYVGWLCWGRLMYVMSPKALKLNLRENELEVLKTAGHLLTREFLRDVTMNLVQ
22B
23A
23B
1640
1660
1680
DNETRGVFSSGNVSFFSLVILLISSGFCELNMSDLFELCESYYNKDDKASMIMSVEIVAG
24A
24B
25A
1700
1720
1740
LVCGSKFMSVSDLDKRDTFIENFLAKCLDYELNHDAFEIWSTLAWWLPAVVDLRRSKTFF
25B
26A
26B
1760
1780
1800
CHFINADGMFDRESDAATHQTSKIYMLRSILMSMEFRAPDVGKLFDELVFDHPYDQVRQA

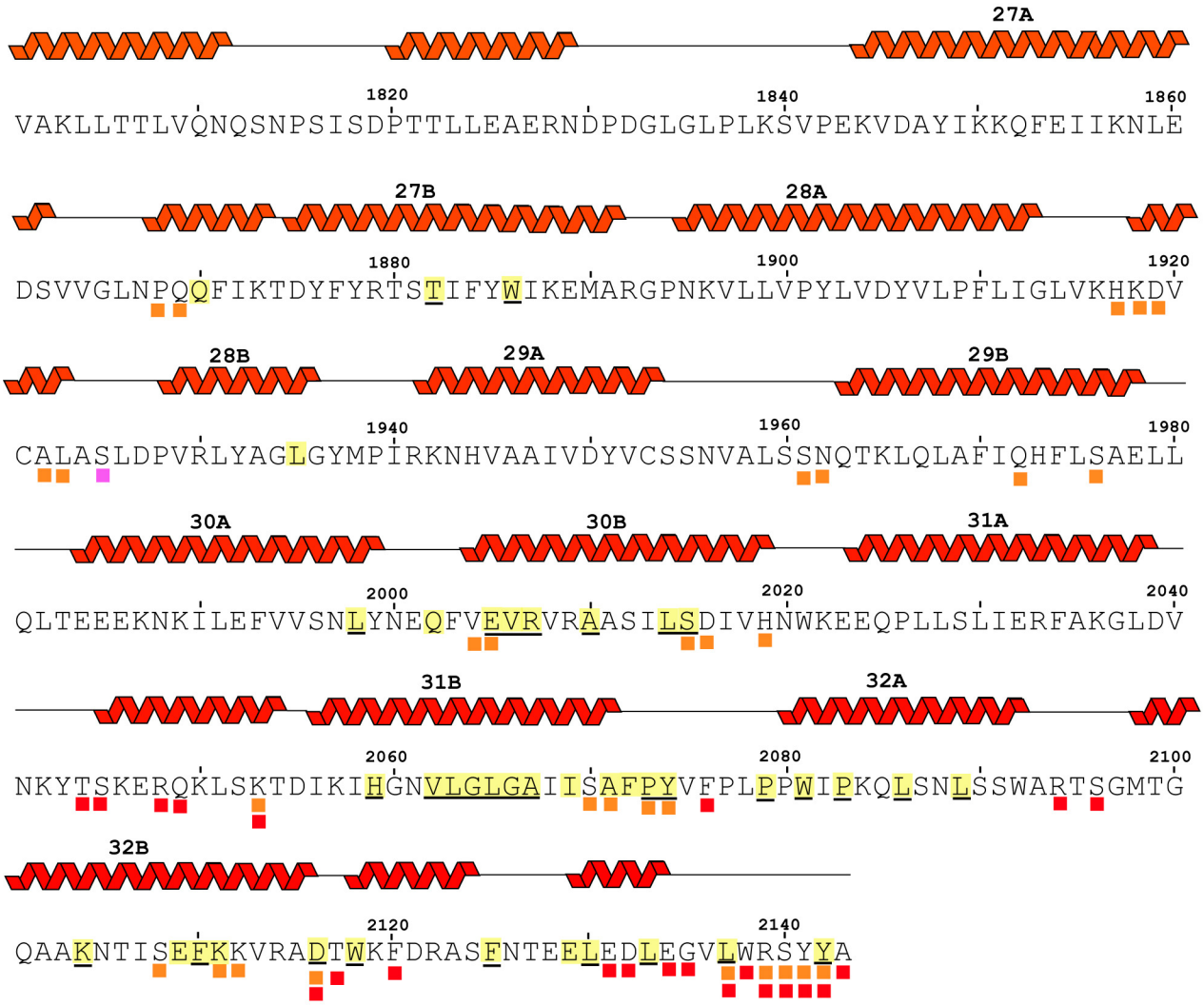
27A
1820
1840
1860
VAKLLTTLVQNQSNPSISDPTTLLEAERNDPDGLGLPLKSVPEKVDAYIKKQFEIIKNLE
27B
28A
1880
1900
1920
DSVVGLNPQQFIKTDYFYRTSTIFYWIKEMARGPNKVLLVPYLVDYVLPFLIGLVKHKDV
28B
29A
29B
1940
1960
1980
CALASLDPVRLYAGLGYMPIRKNHVAAIVDYVCSSNVALSSNQTKLQLAFIQHFLSAELL
30A
30B
31A
2000
2020
2040
QLTEEEKNKILEFVVSNLYNEQFVEVRVRAASILSDIVHNWKEEQPLLSLIERFAKGLDV
31B
32A
2060
2080
2100
NKYTSKERQKLSKTDIKIHGNVLGLGAIISAFPYVFPLPPWIPKQLSNLSSWARTSGMTG
32B
2120
2140
QAAKNTISEFKKVRADTWKFDRASFNTEELEDLEGVLWRSYYA

The 46 sequences used in the alignment to define conserved residues:

gi|37362646|ref|NP_116648.2| [Saccharomyces cerevisiae]
gi|156844582|ref|XP_001645353.1| [Vanderwaltozyma polyspora]
gi|50287269|ref|XP_446064.1| [Candida glabrata]
gi|45201074|ref|NP_986644.1| [Ashbya gossypii]
gi|50308975|ref|XP_454493.1|[Kluyveromyces lactis]
gi|50426149|ref|XP_461671.1| [Debaryomyces hansenii]
gi|150865341|ref|XP_001384517.2|[Pichia stipitis]
gi|68479947|ref|XP_716023.1| [Candida albicans]
gi|149239843|ref|XP_001525797.1|[Lodderomyces elongisporus]
gi|190348667|gb|EDK41164.2| [Pichia guilliermondii]
gi|50551363|ref|XP_503155.1|[Yarrowia lipolytica]
gi|67538874|ref|XP_663211.1|[Aspergillus nidulans]
gi|145257943|ref|XP_001401896.1| [Aspergillus niger]
gi|164425515|ref|XP_960116.2|[Neurospora crassa OR74A]
gi|171682604|ref|XP_001906245.1|[Podospora anserina]
gi|46124079|ref|XP_386593.1|[Gibberella zeae]
gi|154287488|ref|XP_001544539.1|[Ajellomyces capsulatus]
gi|154312206|ref|XP_001555431.1|[Botryotinia fuckeliana]
gi|156064295|ref|XP_001598069.1| [Sclerotinia sclerotiorum]
gi|169606348|ref|XP_001796594.1|[Phaeosphaeria nodorum]
gi|145607561|ref|XP_361868.2|[Magnaporthe grisea]
gi|119194335|ref|XP_001247771.1|[Coccidioides immitis]
gi|121707973|ref|XP_001271992.1|[Aspergillus clavatus]
gi|115391253|ref|XP_001213131.1|[Aspergillus terreus]
gi|119500344|ref|XP_001266929.1|[Neosartorya fischeri]
gi|169771439|ref|XP_001820189.1|[Aspergillus oryzae]
gi|70993706|ref|XP_751700.1|[Aspergillus fumigatus]
gi|189193275|ref|XP_001932976.1| [Pyrenophora tritici-repentis]
gi|170086077|ref|XP_001874262.1| [Laccaria bicolor S238N-H82]
gi|170084821|ref|XP_001873634.1| [Laccaria bicolor S238N-H82]
gi|195997553|ref|XP_002108645.1| [Trichoplax adhaerens]
gi|149449017|ref|XP_001517136.1| [Ornithorhynchus anatinus]
gi|126304432|ref|XP_001382168.1| [Monodelphis domestica]
gi|189524182|ref|XP_001333755.2| [Danio rerio]
gi|73970154|ref|XP_531823.2| [Canis familiaris]
gi|194220729|ref|XP_001497130.2| [Equus caballus]
gi|119903486|ref|XP_606554.3| [Bos taurus]
gi|163644283|ref|NP_055429.2| [Homo sapiens]
gi|66801317|ref|XP_629584.1| [Dictyostelium discoideum AX4]
gi|147906041|ref|NP_001084866.1| [Xenopus laevis]
gi|158290777|ref|XP_312339.4| [Anopheles gambiae str. PEST]
gi|91083491|ref|XP_972018.1| [Tribolium castaneum]
gi|149044860|gb|EDL98046.1| [Rattus norvegicus]
gi|117956381|ref|NP_598774.2| [Mus musculus]
gi|170055259|ref|XP_001863503.1| [Culex pipiens quinquefasciatus]
gi|157110835|ref|XP_001651267.1| [Aedes aegypti]

Figure S2, related to Figure 2B

This is the same as Figure 2B but also includes the closed conformation. Proteasome as seen in: Blm10 complex, white; PA26 complex (pdb 1z7q), yellow; unliganded proteasome (pdb 1ryp), cyan. Residues of the unliganded proteasome and proteasome in the Blm10 complex are labeled if they adopt conformations that are substantially different from that seen in the fully open conformation of the PA26 complex. N-terminal residues are disordered for α2, α3, and α4 in the Blm10 complex.

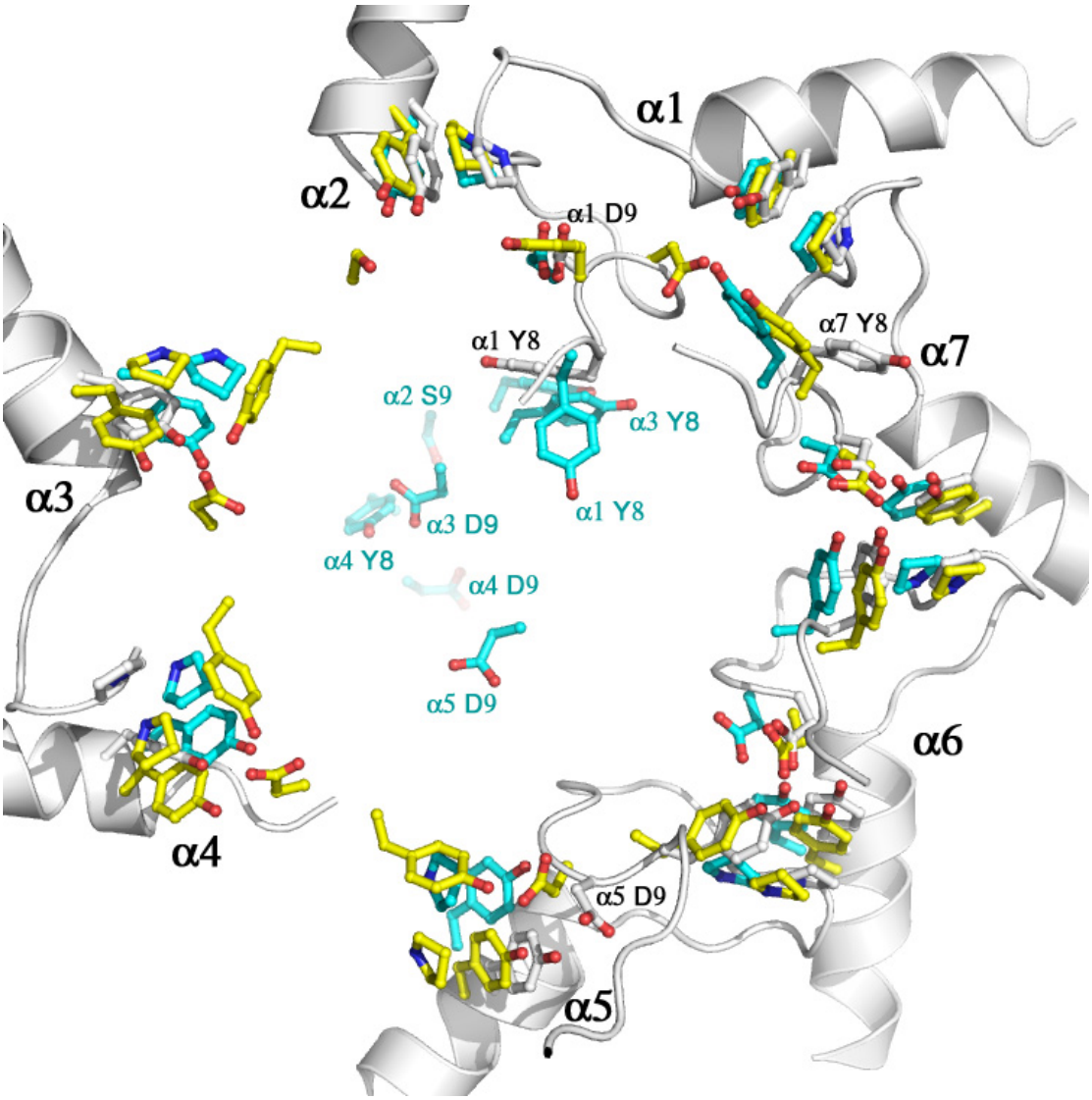

Figure S3, related to Figure 4

(A) Blm10 functions in a proteasome-dependent process

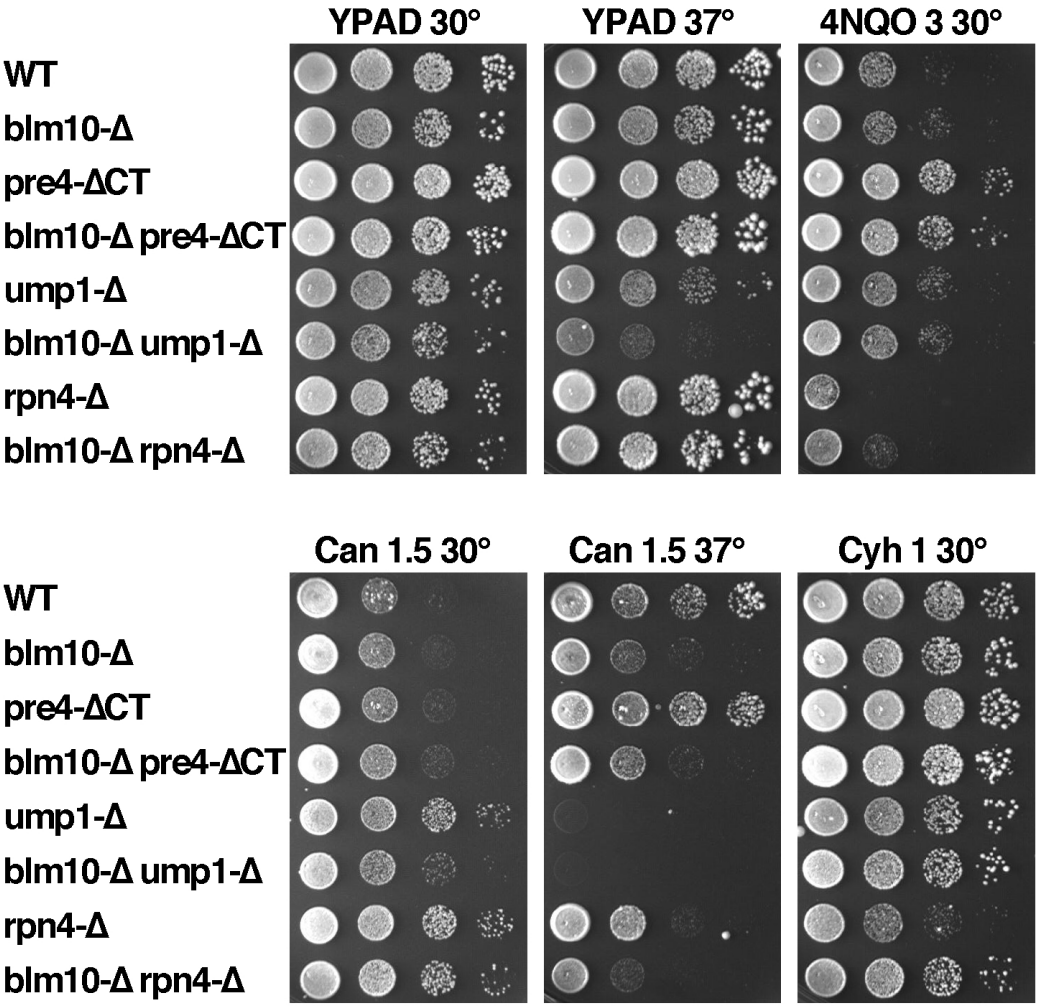

In our experiments using several strain backgrounds, loss of Blm10 did not cause significant sensitivity to any of a number of DNA damaging agents (Iwanczyk et al., 2006). Published reports indicated a role for Blm10 in the assembly or maintenance of 20S proteasomes (Fehlker et al., 2003; Marques et al., 2007), so we tested *blm10*-Δ mutants for defects associated with proteasome deficiency. Strains in the A364a background were grown to saturation in rich medium, then aliquots of 10-fold dilutions were placed on the media indicated and incubated at the temperature indicated in each panel. YPAD is rich medium, 4NQO 3 is YPAD with 3 µg/ml 4-nitroquinoline 1-oxide, Can 1.5 is synthetic medium lacking arginine and containing1.5 µg/ml canavanine, and Cyh 1 is YPAD with 1 µg/ml cycloheximide.

Elevated temperatures or inclusion of the arginine analog canavanine can stress the proteolytic system in yeast by increasing the level of unfolded or aberrantly formed proteins. For example, loss of the 20S assembly chaperone Ump1 caused slow growth at 37° (row 5, YPAD 37°). While neither elevated temperature nor canavanine alone caused a noticeable defect in growth for a *blm10*-Δ mutant, growth on a low level of canavanine at 37° was significantly impaired (compare *blm10*-Δ with WT on the 1.5 μg/ml canavanine plate incubated at 37°). Further, combining both *blm10*-Δ and *ump1*-Δ deletions caused an enhanced growth defect relative to the *ump1*-Δ strain on YPAD at 37°. These observations demonstrate that cells lacking Blm10 have impaired ability to respond to proteolytic stress, possibly due to inadequate proteasome assembly.

It was recently reported that combining *blm10*-Δ with a deletion of the C-terminal 19 residues of the 20S subunit Pre4 (β7) caused strong temperature sensitivity (Marques et al., 2007). We have been unable to reproduce this result using strains in the A364a background, as single and double mutants each grew at equivalent rates at 37° (rows 3 and 4 in the figure) or at 38° (not shown), the maximal permissive temperature for this strain background. To determine whether this difference is due to the different strain backgrounds used, we obtained the strains used by Marques et al. (2007) in the JD47-13c background. After switching the mating type of one strain we performed a genetic cross to generate double *blm10*-Δ *pre4*-Δ*CT* mutants by segregation, instead of the procedure described previously that involved sequential integration of mutations (Marques et al., 2007). Once again, none of the double mutants isolated from the cross displayed temperature sensitivity. Because the *pre4*-Δ*CT* allele used by Marques et al. was not marked, we scored it using a PCR test and verified a subset of the results by DNA sequencing. To further confirm this result, we introduced a similar *pre4*-Δ*CT* mutation into JD47-13c but this time with the *URA3* gene inserted adjacent to the deletion. This allowed a much larger number of double mutant *blm10*-Δ *pre4*-Δ*CT* segregants to be identified and tested, but all of these also proved to be temperature resistant. We were therefore unable to observe a synthetic growth defect or temperature sensitivity for *blm10*-Δ *pre4*-Δ*CT* combinations in either of two genetic strain backgrounds. The pre4-ΔCT strains we constructed in the A364a background do display resistance to 4-nitroquinoline 1-oxide, a phenotype associated with several proteasome assembly defects (Le Tallec et al., 2007), consistent with suboptimal proteasome formation. However, this phenotype is also unaffected by loss of Blm10 (compare rows 3 and 4).

While the results above are consistent with a role for Blm10 in promoting proteasome function, note that genetic analysis of proteasomal assembly and function pathways can be difficult to interpret. For example, Ump1 is needed for normal growth during the proteolytic stress associated with elevated temperature as revealed by weak growth at 37°, but an *ump1*-Δ mutant was more resistant than a WT strain to a different proteolytic stress, the presence of a low level of canavanine (compare rows 1 and 5 in the canavanine 1.5 at 30° panel). Rpn4 is a transcription factor that upregulates proteasome gene expression under conditions of proteolytic stress (Mannhaupt et al., 1999; Xie and Varshavsky, 2001), but an *rpn4*-Δ mutant grows normally at 37°, is sensitive to 4NQO, and in our tests is more resistant than WT to canavanine at 30° but more sensitive than WT to canavanine at 37°. Unlike the *pre4*-Δ*CT* or *ump1*-Δ strains, the *rpn4*-Δ mutant is sensitive to the protein synthesis inhibitor cycloheximide (Cyh). Loss of Blm10 suppressed this defect and the 4NQO sensitivity, but enhanced the defect in growth observed for the *rpn4*-Δ strain on canavanine at 37°. Schmidt et al. (2005) found that *rpn4*-Δ caused slight sensitivity to canavanine and that *rpn4*-Δ *blm10*-Δ double mutants had a slight synthetic growth defect both on rich medium and on canavanine. These results differ from ours, possibly due to strain background differences. Alternatively, as we have found that *blm10*-Δ mutants lose mitochondrial function at a high frequency, perhaps some of the variation among different experiments can be accounted for by clonal variation. That is, different cultures will have different retention of mitochondrial function due to the stochastic nature of the loss, contributing to phenotypic variation among cultures in a given assay even when comparing different clones of the same strain.

Together these results are consistent with a role for Blm10 in a proteasome-dependent process, but they illustrate the difficulty of interpreting genetic effects when examining a factor like the proteasome that directly or indirectly alters many facets of a broad range of physiologically important processes.

(B). Loss of *BLM10* has minor effects on ROS formation and mitochondrial genome mutation

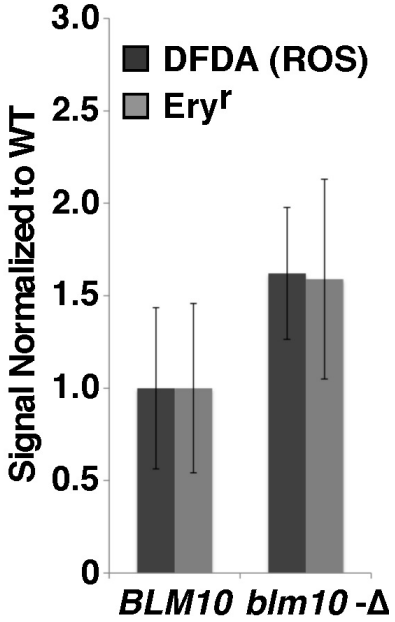

Isogenic strains with or without *BLM10* (8127-7-4, 8634-9-1) were grown to log phase in rich medium and then tested for production of reactive oxygen species (ROS) or mutation of the mitochondrial genome as detected by production of erythromycin resistant clones, essentially as described (Malc et al., 2009). Briefly, for the ROS assay, cells were collected by centrifugation, washed, then multiple aliquots were suspended in a solution containing 10 μM 2', 7'-Dichlorofluorescein diacetate (Sigma, DFDA). After incubating 30 minutes at 30° the cells were washed again, suspended in detergent and lysed by agitation with glass beads. The fluorescence of the supernatant was then tested at 520 nm with excitation at 485 nm. Signal in this assay depends on the intracellular level of ROS (Doudican et al., 2005). Dilutions of the same cultures were plated on rich medium with glycerol as the sole carbon source and containing 4 mg/ml of erythromycin. The yield of erythromycin resistant clones was then determined as an indication of the frequency of mutation of the mitochondrial rDNA locus, which determines sensitivity to this antibiotic. Three independent cultures were tested in each assay, normalized to the value obtained for the WT samples, and the average and standard deviation (error bars) presented here. The average values for the WT were 1.4 fluorescence units/A660 value, and 24 erythromycin resistant colonies per 10^7 viable cells on glycerol medium lacking the drug. Loss of *BLM10* in this and other assays consistently caused slightly higher levels of ROS production and mitochondrial genome mutation, but the effect is small and not statistically significant in any single assay.

(C) Western blot showing the stability of Blm10-CTΔ3

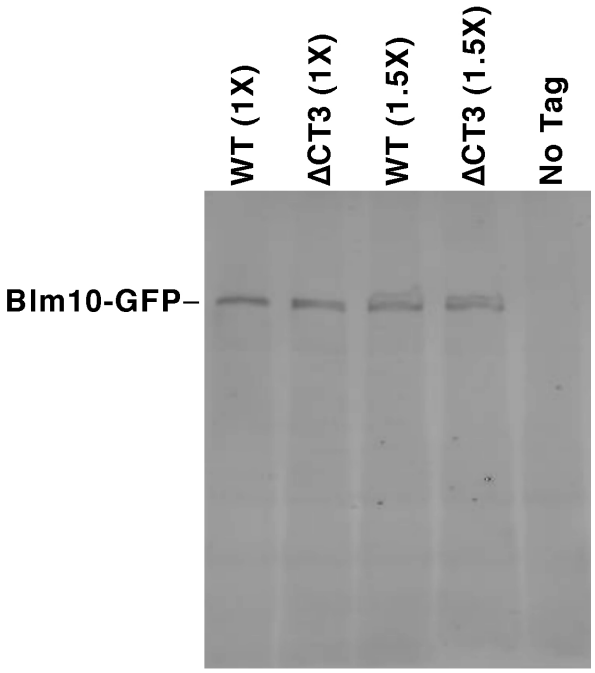

Strains 8670-1134 (WT Blm10 with GFP inserted after residue 1134), 8675-1134 (the same but with the last three residues of the Blm10 ORF deleted), and a related strain without a GFP tag were grown to log phase, treated with trichloroacetic acid, and processed for SDS-PAGE and western blotting as described (VanDemark et al., 2008). GFP was detected with a monoclonal antibody against this protein. The band indicated is the full-length fusion protein. This shows that neither deletion of the last three residues of Blm10 nor insertion of the *URA3* gene downstream of the Blm10 ORF cause detectable changes in the level of Blm10 protein. (Hua Xin, personal communication).

Table S1. Strains used, related to Figure 4

Strains were constructed using standard methods. JD47-13c and AM36 were obtained from J. Dohman (Marques et al., 2007). The final 3 residues of Blm10 were deleted by transforming with a PCR product generated using pRS406 (Brachmann et al., 1998; Longtine et al., 1998) as the template and an oligonucleotide that replaces the first tyrosine in the C-terminal ...YYA sequence with a stop codon followed by the normal 30 bp of genomic sequence found downstream of the *BLM10* gene. This inserts the URA3 gene 30 bp downstream of a C-terminally deleted allele in an otherwise normal genomic context, as confirmed by sequencing. Similar strategies were used to mark WT *BLM10* in the same position, to delete the final residue of the ORF, and to mutate the final YYA sequence to AAA.

Strain	Used in	Mating type	Genotype
A364a genetic background:			
2268-1-1	Fig 5	*MATa*	*ura3-Δ0 leu2-Δ0 trp1-Δ2 his7 blm10-Δ(::LEU2)*
7860-6-4	Fig 5	*MATa*	*ura3-Δ0 leu2-Δ0 trp1-Δ2 his7*
8015-4-1	Fig 5	*MATa*	*ura3-Δ0 leu2-Δ0 trp1-Δ2 his7 blm10-Δ(::TRP1)*
8127-5-1	Fig 5	*MATa*	*ura3-Δ0 leu2-Δ0 trp1-Δ2 his7 lys2-128∂*
8127-5-2	Fig S2	*MATa*	*ura3-Δ0 leu2-Δ0 trp1-Δ2 his3 lys2-128∂*
8127-7-4	Fig 5, S4	*MATa*	*ura3-Δ0 leu2-Δ0 trp1-Δ2 his3 lys2-128∂*
8130-1	Fig 5	*MATa*	*ura3-Δ0 leu2-Δ0 trp1-Δ2 his7 blm10-Δ(::KanMX)*
8151-1-1	Fig 5	*MATa*	*ura3-Δ0 leu2-Δ0 trp1-Δ2 his7 lys2-128∂*
8386-7-2	Fig 5	*MATa*	*ura3-Δ0 leu2-Δ0 trp1-Δ2 his7 lys2-128∂*
8571-2-1	Fig S2	*MATa*	*ura3-Δ0 leu2-Δ0 trp1-Δ2 his3 lys2-128∂ pre4-CTΔ19(URA3)*
8574-1-3	Fig S2	*MATa*	*ura3-Δ0 leu2-Δ0 trp1-Δ2 his3 lys2-128∂ rpn4-Δ(::KanMX)*
8577-6-1	Fig 5	*MATa*	*ura3-Δ0 leu2-Δ0 trp1-Δ2 his7 lys2-128∂ blm10-Δ(::LEU2)*
8578-2-4	Fig S2	*MATa*	*ura3-Δ0 leu2-Δ0 trp1-Δ2 his3 lys2-128∂ blm10-Δ(::LEU2) rpn4-Δ(::KanMX)*
8578-7-1	Fig S2	*MATa*	*ura3-Δ0 leu2-Δ0 trp1-Δ2 his3 lys2-128∂ blm10-Δ(::LEU2)*
8579-6-3	Fig 5	*MATa*	*ura3-Δ0 leu2-Δ0 trp1-Δ2 his7 lys2-128∂ blm10-Δ(::LEU2)*
8583-2-1	Fig S2	*MATa*	*ura3-Δ0 leu2-Δ0 trp1-Δ2 his3 lys2-128∂ blm10-Δ(::LEU2) pre4-CTΔ19(URA3)*
8628-1-1	Fig 5	*MATa*	*ura3 leu2 trp1 his3 lys2-128∂ blm10-CTΔ3(URA3)*
8634-9-1	Fig 5, S4	*MATa*	*ura3-Δ0 leu2-Δ0 trp1-Δ2 his3 lys2-128∂ blm10-Δ(::LEU2)*
8647-9-2	Fig 5	*MATa*	*ura3 leu2 trp1 his7 lys2-128∂ blm10-Δ(::KanMX)*
8664-1-3	Fig 5	*MATa*	*ura3 leu2 trp1 his7 lys2-128∂ blm10-CTΔ3(URA3)*
8685	Fig 5	*MATa*	*ura3-Δ0 leu2-Δ0 trp1-Δ2 his7 lys2-128∂ blm10-YYA2141-2143AAA(URA3)*
8670-1134	Fig S5	*MATa*	*ura3-Δ0 leu2-Δ0 trp1-Δ2 his7 lys2-128∂ BLM10(1134-GFP)*
8675-1134	Fig S5	*MATa*	*ura3-Δ0 leu2-Δ0 trp1-Δ2 his7 lys2-128∂ blm10-ΔCT3(1134-GFP, URA3)*
8688	Fig 5	*MATa*	*ura3-Δ0 leu2-Δ0 trp1-Δ2 his7 lys2-128∂ blm10-*2144A(URA3)*
8689	Fig 5	*MATa*	*ura3-Δ0 leu2-Δ0 trp1-Δ2 his7 lys2-128∂ blm10-CTΔ1(URA3)*
8690	Fig 5	*MATa*	*ura3-Δ0 leu2-Δ0 trp1-Δ2 his7 lys2-128∂ BLM10(URA3)*

S288c genetic background

8266-7-5a	Fig 5	*MATa*	*leu2-Δ1 trp1-Δ63 ura3-52 his4-912∂ lys2-128∂*
8358-T1	Fig 5	*MATa*	*leu2-Δ1 trp1-Δ63 ura3-52 his4-912∂ lys2-128∂ blm10-Δ(::TRP1)*

W303 genetic background

8025-2-3	Fig 5	*MATa*	*ade2 can1 his3 ura3 leu2 trp1 adh4:URA3*
8132	Fig 5	*MATa*	*ade2 can1 his3 ura3 leu2 trp1 adh4:URA3 blm10-Δ(::TRP1)*

JD47-13c genetic background

JD47-13c	Fig 5	*MATa*	*his3-Δ200 leu2-3,112 lys2-801 trp1-Δ63 ura3-52*
AM36	Fig 5	*MATa*	*his3-Δ200 leu2-3,112 lys2-801 trp1-Δ63 ura3-52 blm10-Δ(::KanMX4)*

Supplemental Experimental Procedures

Protein Preparation

Double capped *S. cerevisiae* proteasome:Blm10 and proteasome:Δ50Blm10 complexes were prepared largely as described (Iwanczyk et al., 2006). Briefly, *S. cerevisiae* strain SDL135 expressing proteasome subunit Pre1/β4 tagged with protein A at the C-terminus (Leggett et al., 2002) (kind gift of Daniel Finley and David Leggett) was grown in a 36 L fermentor in YPD+glucose at 30°C for 2 days to saturation, and harvested by centrifugation. Polyhistidine-tagged Blm10 was expressed from pTF155/pCPH1327 (full length) or pCPH1328 (Δ50) in a 36L fermentor or shaker flasks in synthetic medium with raffinose to an OD^{600} of 0.7 at 30°C, whereupon expression was induced by the addition of galactose to 1.1% and the culture grown overnight and harvested by centrifugation. Cell lysis was performed under liquid nitrogen using a freezer mill 6850 pulverizor (SPEX CentriPrep Group). Subsequent steps were performed at 4°C. Typical preparations started with 80g of cell paste expressing tagged proteasome and 80g of cell paste expressing Blm10, and followed the published protocol (Iwanczyk et al., 2006) to give a typical yield of 2-4 mg of complex. Protein was concentrated to 20-25 mg/ml in 50mM Tris pH 7.5, 50mM NaCl, 1mM EDTA, and 0.5mM dithiothreitol (DTT) using a spin filtration device. The concentrated protein was buffer exchanged in the same solution with fresh DTT using a G50-sephadex spin column.

Crystallization

Immediately prior to setting up crystallization trials, the protein sample was centrifuged at 16,000 *g* at 4°C for 10 minutes. Blm10:proteasome complex crystals were grown by vapor diffusion in drops comprising 0.5μL protein and 0.5μL reservoir against a reservoir of 5-6% PEG 8k, 0.1M Na/K phosphate pH 6.2, 0.2M NaCl, and 18-30% of ethylene glycol. Crystals were harvested by addition of ~50 μL of well solution to the drop immediately prior to suspending the crystal in a nylon loop and plunging into liquid nitrogen. Crystals with full-length Blm10 and Blm10 missing the first 50 amino acid residues (Blm10Δ50) grew under the same conditions and generally had similar morphologies, although the Blm10Δ50 complex crystals grew more reproducibly in about 2-3 weeks and diffracted more strongly. Growth of full-length Blm10 complex crystals took from weeks to months and was highly non-reproducible, with the large majority of preparations not yielding usable crystals. Both of the constructs had N-terminal extensions of 12 histidine residues, and started with the sequence H_{12}-G-

T^2 or H_{12}-GT-D^{51}. The polyhistidine tags were not removed prior to setting up crystallization trials. The full-length Blm10:proteasome crystals were poorly isomorphous and showed large variation in cell dimensions and even in space group.

Structure Determination

Diffraction data were collected at the National Synchrotron Light Source beamline X29 and processed using HKL (Otwinowski and Minor, 1997). Data were collected from the various crystals (Table 1) at 100K and at the wavelength indicated: c158 1.1 Å; c164 1.0 Å; c172 1.0688 Å; c280 1.0809 Å; c290 1.0 Å; c292 1.0642 Å. Many of the crystallographic calculations were performed using programs of the CCP4 suite (Collaborative Computational Project, 1994). The various crystal forms were phased by molecular replacement with PHASER (McCoy et al., 2007) using the unliganded structure of the *S. cerevisiae* proteasome (Groll et al., 1997) (pdb code 1ryp) as the search model. Map quality was greatly improved by non-crystallographic symmetry (NCS) averaging over the multiple copies of half proteasome:Blm10 complexes in the asymmetric unit and averaging between different crystal forms using DMMULTI (Cowtan, 1994). Map quality was further improved by application of a -50 $Å^2$ sharpening factor. Crystals belonging to space group $P2_1$ had four-fold NCS, and crystals belonging to space group $P2_12_12_1$ had two-fold NCS.

Model building with O (Jones et al., 1991) was aided by the identification of 20 methionine and 14 cysteine sites from crystals soaked in thimerosal, methyl mercury nitrate, or potassium platinum tetrachloride. Heavy atom derivates were prepared by adding aqueous stock solutions to the crystallization well solution to make the concentration indicated, followed by addition of 40 μL of this solution directly to the crystallization drop for the time indicated prior to mounting and plunging into liquid nitrogen: c164/FL-Thim, thimerosal, 6mM, 2 hours; c172/FL- $PtCl_4$, 6 mM, 2 hours; c290/Δ50-MeHg, $MeHgNO_2$, 1 mM, 10 minutes; c292/Δ50-$PtCl_4$, K2PtCl4 2mM, 24 hours. Due to non-isomorphism, the heavy atom derivative structures were determined individually by molecular replacement and their phases refined by NCS averaging. Anomalous difference Fourier maps were found to be more sensitive than isomorphous difference maps for the location of heavy atoms.

The best diffracting crystal structure was refined with REFMAC5 (Murshudov et al., 1997) and rebuilt with KiNG (Davis et al., 2007), with the final refinement calculations performed using Phenix (Adams

et al., 2002). All measured reflections (except the test set) were used in refinement, regardless of I/σ(I) value, up to a Bragg spacing of 3.0 Å, at which point the σ_A value falls precipitously (DeLaBarre and Brunger, 2006). No solvent molecules were included in the model. NCS restraints were set automatically in Phenix and only minor deviations from NCS are apparent. Stereochemistry was assessed using MolProbity (Davis et al., 2007), and the overall clashscore was 70% for the Blm10 portion of the structure in comparison with other structures reported at 3.4 Å resolution. The clashscore was 89% for the proteasome portion of the structure. Molprobity evaluated 87.8% of residues as possessing favored Ramachandran angles and 2.8% as being outliers. The following residues lacked defined density and have been omitted from the model. Blm10: N-terminus to Ser78, Asp155-Ala238, Arg1038-Asp1146. Proteasome: α1 before Ala10, α2 before Gln20, α3 before Ser14, α4 before Ile17, α7 before Gly4. All other proteasome residues that were present in the search model were also included in the Blm10 complex refinement. Crystallographic statistics are given in Table 1. The figures were made with PyMol (DeLano, 2002).

Supplemental References

Adams, P.D., Grosse-Kunstleve, R.W., Hung, L.W., Ioerger, T.R., McCoy, A.J., Moriarty, N.W., Read, R.J., Sacchettini, J.C., Sauter, N.K., and Terwilliger, T.C. (2002). PHENIX: building new software for automated crystallographic structure determination. Acta Crystallogr D Biol Crystallogr *58*, 1948-1954.

Brachmann, C.B., Davies, A., Cost, G.J., Caputo, E., Li, J., Hieter, P., and Boeke, J.D. (1998). Designer deletion strains derived from Saccharomyces cerevisiae S288C: a useful set of strains and plasmids for PCR-mediated gene disruption and other applications. Yeast *14*, 115-132.

Collaborative Computational Project, N. (1994). The CCP4 suite: programs for protein crystallography. Acta Crystallogr D Biol Crystallogr *50*, 760-763.

Cowtan, K.D. (1994). 'dm': An automated procedure for phase improvement by density modification. Joint CCP4 and ESF-EACBM newsletter on protein crystallography *31*, 34-38.

Davis, I.W., Leaver-Fay, A., Chen, V.B., Block, J.N., Kapral, G.J., Wang, X., Murray, L.W., Arendall, W.B., 3rd, Snoeyink, J., Richardson, J.S.*, et al.* (2007). MolProbity: all-atom contacts and structure validation for proteins and nucleic acids. Nucleic Acids Res *35*, W375-383.

DeLaBarre, B., and Brunger, A.T. (2006). Considerations for the refinement of low-resolution crystal structures. Acta Crystallogr D Biol Crystallogr *62*, 923-932.

DeLano, W.L. (2002). The PyMOL Molecular Graphics System (DeLano Scientific, San Carlos, CA, USA.).

Doudican, N.A., Song, B., Shadel, G.S., and Doetsch, P.W. (2005). Oxidative DNA damage causes mitochondrial genomic instability in Saccharomyces cerevisiae. Mol Cell Biol *25*, 5196-5204.

Gouet, P., Courcelle, E., Stuart, D.I., and Metoz, F. (1999). ESPript: analysis of multiple sequence alignments in PostScript. Bioinformatics *15*, 305-308.

Jones, T.A., Zou, J.Y., Cowan, S.W., and Kjeldgaard, M. (1991). Improved methods for building protein models in electron density maps and the location of errors in these models. Acta Crystallogr A *47 (Pt 2)*, 110-119.

Le Tallec, B., Barrault, M.B., Courbeyrette, R., Guerois, R., Marsolier-Kergoat, M.C., and Peyroche, A. (2007). 20S proteasome assembly is orchestrated by two distinct pairs of chaperones in yeast and in mammals. Mol Cell *27*, 660-674.

Leggett, D.S., Hanna, J., Borodovsky, A., Crosas, B., Schmidt, M., Baker, R.T., Walz, T., Ploegh, H., and Finley, D. (2002). Multiple associated proteins regulate proteasome structure and function. Mol Cell *10*, 495-507.

Longtine, M.S., McKenzie, A., 3rd, Demarini, D.J., Shah, N.G., Wach, A., Brachat, A., Philippsen, P., and Pringle, J.R. (1998). Additional modules for versatile and economical PCR-based gene deletion and modification in Saccharomyces cerevisiae. Yeast *14*, 953-961.

Mannhaupt, G., Schnall, R., Karpov, V., Vetter, I., and Feldmann, H. (1999). Rpn4p acts as a transcription factor by binding to PACE, a nonamer box found upstream of 26S proteasomal and other genes in yeast. FEBS Lett *450*, 27-34.

McCoy, A.J., Grosse-Kunstleve, R.W., Adams, P.D., Winn, M.D., Storoni, L.C., and Read, R.J. (2007). Phaser crystallographic software. J Appl Cryst *40*, 658-674.

Murshudov, G.N., Vagin, A.A., and Dodson, E.J. (1997). Refinement of macromolecular structures by the maximum-likelihood method. Acta Crystallogr D Biol Crystallogr *53*, 240-255.

Ortega, J., Heymann, J.B., Kajava, A.V., Ustrell, V., Rechsteiner, M., and Steven, A.C. (2005). The axial channel of the 20S proteasome opens upon binding of the PA200 activator. J Mol Biol *346*, 1221-1227.

Otwinowski, Z., and Minor, W. (1997). Processing of X-ray diffraction data collected in oscillation mode. Methods Enzymol *276*, 307-326.

VanDemark, A.P., Xin, H., McCullough, L., Rawlins, R., Bentley, S., Heroux, A., Stillman, D.J., Hill, C.P., and Formosa, T. (2008). Structural and functional analysis of the Spt16p N-terminal domain reveals overlapping roles of yFACT subunits. J Biol Chem *283*, 5058-5068.

Xie, Y., and Varshavsky, A. (2001). RPN4 is a ligand, substrate, and transcriptional regulator of the 26S proteasome: a negative feedback circuit. Proc Natl Acad Sci U S A *98*, 3056-3061.